(1)

August 1992 THESIS

An Analysis of the Composition of Auroral Emissions in the Near Infrared

Thomas J. Smith, Captain

AFIT Student Attending: University of Michigan AFIT/CI/CIA-92-118

AFIT/CI
Wright-Patterson AFB OH 45433-6583

THE UNIVERSITY OF MICHIGAN
Department of Atmospheric, Oceanic, and Space Sciences
Space Physics Research Laboratory

AN ANALYSIS OF THE COMPOSITION OF AURORAL EMISSIONS IN THE NEAR INFRARED

by

Thomas J. Smith

Supported by:

Air Force Institute of Technology
Air University, United States Air Force

Research Advisor:
Dr. Jeng-Hwa Yee

August 1992

A thesis submitted in partial fulfillment
of the requirement for the degree of
Master of Science
(Atmospheric and Space Sciences)
from the University of Michigan
1992

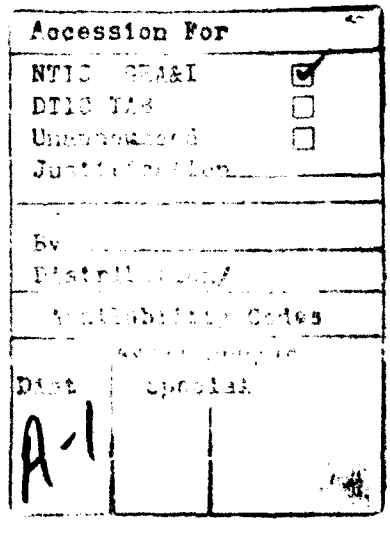

Knowlege is good.

Emil Faber, Founder, Faber College

(from Animal House, ©1980)

To Janet,

ACKNOWLEDGEMENTS

There are many people who I'd like to express sincere gratitude to helping me toward this major achievement in my life. First, and foremost, my wife, Janet, whose unending concern, patience, and caretaking I could not have done without.

On the computing staff, I'd like to thank Gerry Scmitt for his willingness to drop what he's doing to lend a helping hand whenever a computing problem occurred. Much thanks to Dave Steinbach and his staff for assistance in keeping these Macintosh computers in working order.

From the secretarial staff, much thanks goes to Debbie Eddy, Erin Morris, Sue Young, and Carol Quinnell. I'd like to express special thanks to Nelly DeMaldonado for relentless assistance whenever I needed it. I always knew I could count on her.

Thanks to the AFIT graduate students who have helped along the way: Ed Hume, Pat Purcell, Jerry Davis, and Steve Carr. Other students at SPRL who have been a great help are: Eric Buscela for the use and assistance in the use of his BANDSYN model, Matt Turnbull for his great help in the use of his Fabry-Perot interferometer for a study in AOSS 495, and also appreciation to Ken Fischer, Lynn Thomas, Linnea Nooden, Matt McGill, Donliang Wu, and Ned Snell.

Last, but certainly not least, my highest regards to my research advisor, Dr. Jeng-Hwa (Sam) Yee, for his willingness to come to the rescue at the drop of a hat, and always expert advice, which is equalled by no one

else I've worked for. Also thanks to my parents, Manson and Joan Smith, for their support through all the years of my life. Thanks to my children, Matt, Chris, and Michelle for enduring the many moves associated with this degree. For the above mentioned and those which may have been unintentionally left out, my sincerest thanks.

TABLE OF CONTENTS

LIST OF FIGURES

LIST OF TABLES

CHAPTER 1

INTRODUCTION

1.1 Background

1.1.1 History of Auroral Science

An excellent description of the history of auroral science was given in a lecture by the great Sydney Chapman at the NATO Advanced Study Institute, held at Ås, Norway, July 29 through August 9, 1968. This summary was derived from the publication of Chapman's and other lectures put together by McCormac and Omholt, in *Atmospheric Emissions*.

Chapman supposed the beginnings of auroral history dated back to 1600, when Gilbert discovered the earth is a great magnet. In 1621 a magnificent auroral display was witnessed by Gassendi from the south of France; he was perhaps the first scientist to view it objectively. He named it the *aurora borealis*, or northern dawn. Nearly a century later, in 1716, Halley was the first to suggest a connection between the aurora and the geomagnetic field, when he observed the great aurora in London.

Also in London, in 1722, Graham discovered the transient variations of the earth's magnetic field, which are regular on some days and disturbed on others. Celsius, with an instrument from Graham, began similar studies in Uppsala, Sweden. By correspondence they found that days disturbed at Uppsala were disturbed also in London. In 1741 Celsius and his assistant Hiorter noted that the occurrence of aurora is linked with magnetic disturbances. Thus, when Gassendi in France and Halley in London saw an aurora, there must have been, unknown to them, what Humboldt in 1806 called a *magnetic storm*. A reasonable estimate of the height of an aurora seen in England in 1784 was made by Cavendish.

In 1833 the geographer Mucke recognized the existence of the auroral zone of maximum frequency of auroral visibility, from his studies of the auroral reports of arctic explorers, and from the long records made by atomic chemist, Dalton. By 1844, Schwabe had recognized the occurrence of the sunspot cycle, and within a decade it was found that the magnetic variations, both regular and enhanced, are more frequent around sunspot maximum. Owing to the poor quality of auroral statistics it took decades before it was established that the aurora also follows the sunspot cycle.

In 1846 the Scottish geophysicist Broun thought horizontal magnetic measurements had a lunar periodicity, but in 1858 he re-interpretted the variation as being connected with the solar rotation. In 1868, Ångstrom made the first observations of the auroral spectrum, the beginning of a great chapter in auroral science, but it's study made little progress in the nineteenth century because of what atomic physicists were yet to discover. In 1882, the Scottish physicist, Stewart, inferred the existence of what we now call the ionosphere, concluding that the dependence of the daily

magnetic variation on the sunspot cycle could only be explained by electric currents in a conducting layer of the upper atmosphere.

The advances toward an auroral *theory* awaited the discovery of the electron by atomic physicists, around 1880, and also on experiments and theory that showed how the electron's motion is affected by magnetic, as well as electric fields. This led Birkeland in 1896 to infer that auroras occur in polar regions because the geomagnetic field must deflect migratory electrons toward those regions. This and other theories were important beginnings in auroral science, and were greatly modified through the years.

One of the most notable areas of auroral study which has made great progress is in spectroscopy of the aurora. Measurement and identification of numerous atomic lines and molecular bands in the auroral spectrum was a great task undertaken by many scientists, and is still ongoing. Though many unknowns still exist, a great deal is known about the aurora, thanks to studies and advances in instrumentation during the 20th century.

1.1.2 Fundamentals of Aurora

Auroral activity, as implied above, has a regional preferrence determined by magnetic latitude. Since the earth's magnetic field approximates a magnetic dipole, corrected dipole latitude is often used instead of geographic latitude. The *auroral zone* is generally accepted to be the region between 60 and 75 degrees IN Lat (dipole latitude), on average. This is the most likely region to contain the *auroral oval*, the area of auroral activity. Ann Arbor, Michigan's dipole latitude is about 53 deg IN, it's

geographic latitude is about 42 N. The IN latitude puts Ann Arbor just outside the *auroral zone* .

Figure 1.1 shows the auroral oval at various levels of magnetic disturbance.

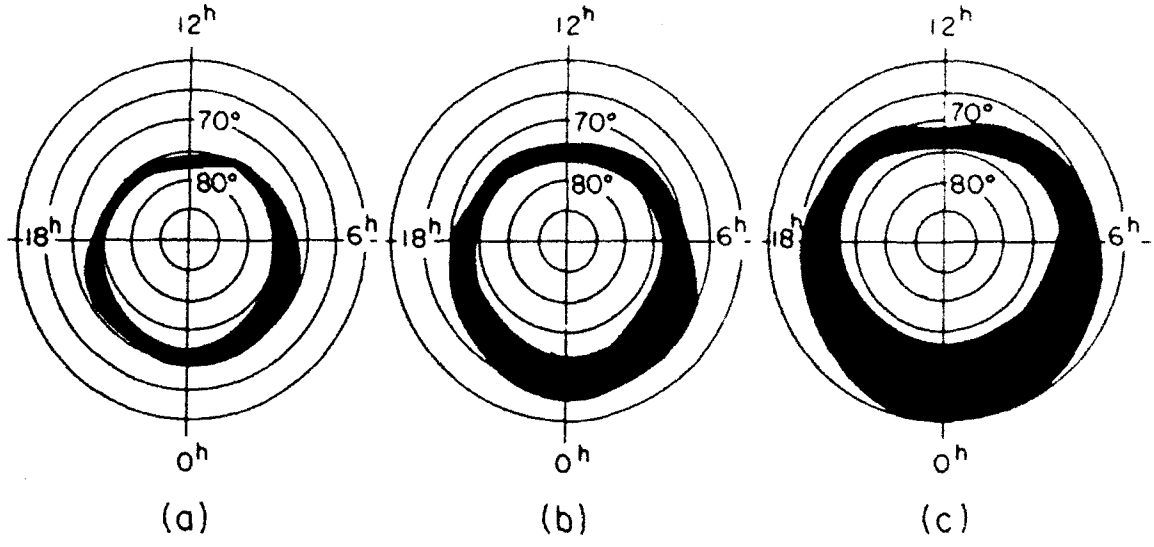

Figure 1.1 Auroral oval for various levels of magnetic disturbance index Q. Cases (a), (b), and (c) are for Q=0,3, and 7 respectively. The mean auroral oval is similar to (b). (after Starkov and Feldstein, 1968).

The reason for the auroral zone's existense can be seen when viewing an illustration of the earth's magnetic field. Figure 1.2 shows the earth's magnetic field and how charged particles migrate in the vicinity of earth, once trapped by it's magnetic field.

As seen in the illustration, charged particles spiral around the magnetic flux lines themselves, while drifting around the earth. When the particles reach a turning point, as illustrated in the figure, they reflect back to the other direction. Thus the trapped particles (presumed to be electrons

here) oscillate back and forth between reflection points as they drift around the globe, to a first approximation.

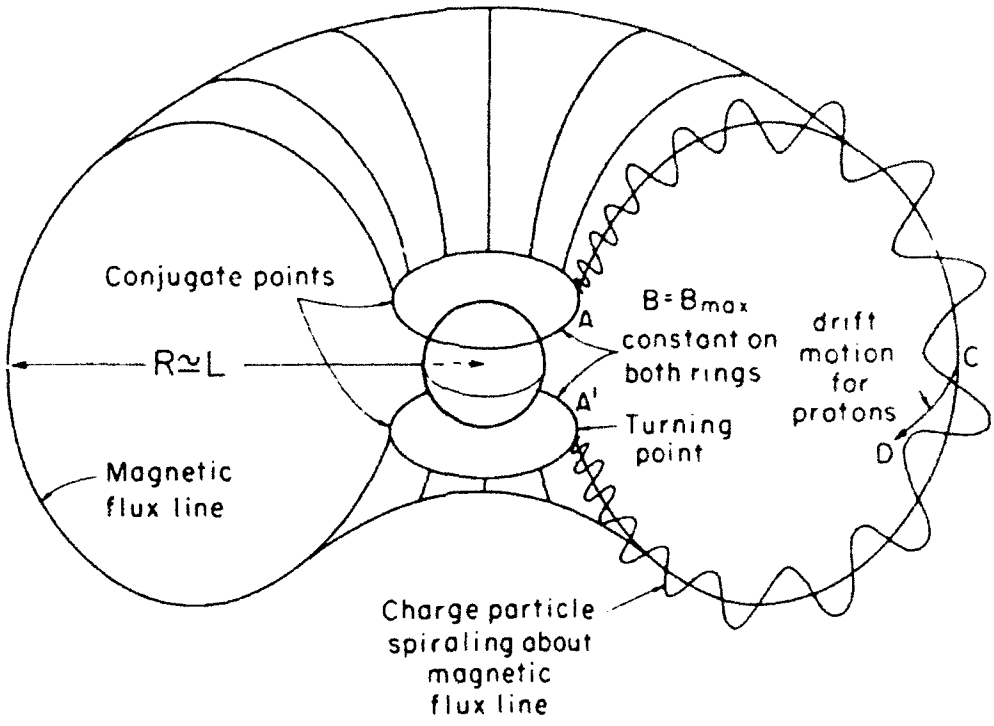

Figure 1.2 Motion of trapped particles in a dipole-like field. (adapted from Whalen et al., 1974).

These electrons are very energetic- they contain many keV's of energy. Compared with the 13.6 eV it takes to ionize an N_2 molecule, it can be seen that this is huge amount of energy, and the energy from a single electron can be distributed to thousands of ambient particles.

The source of these energetic electrons is of course the sun. Solar flares, giant explosions which release fiercely hot particles from the sun, occur more frequently during high sunspot activity, which follows an 11-year cycle. Some of these energetic particles are intercepted by earth's magnetic field and may become trapped by the region, and a portion of them

are steered to the near-earth region, becoming a source of energy for the aurora. Such an event occurred on November 8, 1991.

1.1.3 The November 1991 Measurement

The year of 1991 was an active year for the star which we call the sun. During our sun's well known 11 year cycle, 1991 was one of the peak years of solar activity. On November 8, 1991 solar activity was fairly high, with a 10.7 cm radio wave flux (F10.7) index reading of 200.4, and geomagnetic activity near earth was at severe storm levels, with a planetary magnetic (Ap) index daily average at 65 on November 8, and 99 on November 9. On the evening of the 8th auroral displays were witnessed unusually far equatorward, as far south as Lubbock, Texas in North America. In Ann Arbor, Michigan, the University of Michigan's Near Infrared Spectrometer (NIRS) was operating and measured the auroral display overhead from approximately 6 PM to 12 PM local time, in the spectral region of 8400 to 8900 Å. Frames of the aurora were taken at, and integrated over, 30 second intervals during that time.

Figure 1.3 shows the measured spectra as a function of time. The most obvious features in the graph are the more intense peaks which are attributable to atomic oxygen and atomic nitrogen emission lines. The aurora was brightest near 2000 hrs local standard time (LST), or 8 PM, then after 2100 LST the intensity dropped off remarkably and remained at the much less intense nightglow levels for the rest of the measurement period.

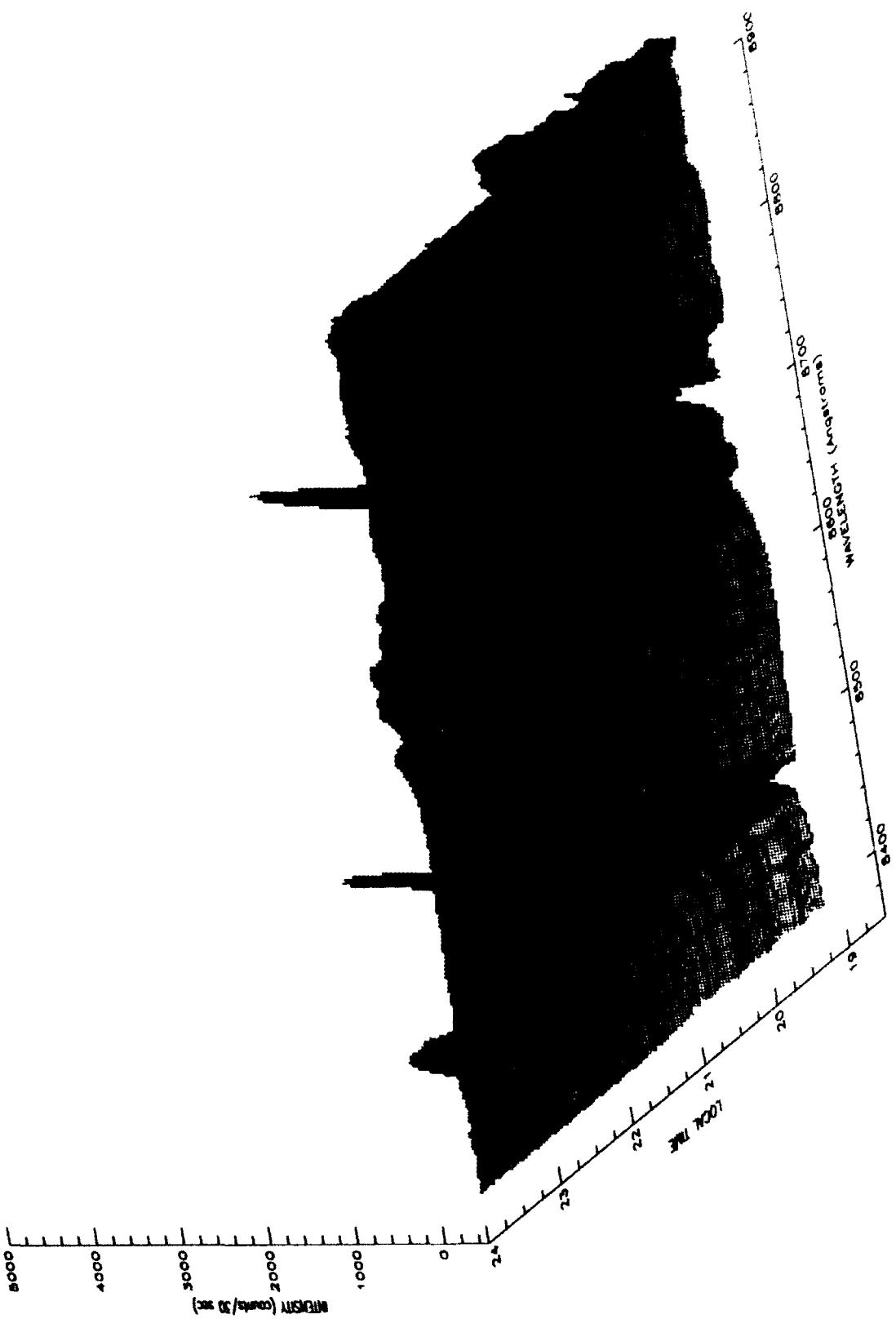

Figure 1.3 Measurement of aurora taken over Ann Arbor, Michigan on November 8, 1991.

1.2 Purpose of Research

The purpose of this research was to analyze the data and determine which atomic and molecular species were responsible for the emissions in the spectral region measured, then determine species brightnesses and molecular band temperatures. This would be accomplished by comparing the calculated spectra with the measured spectra, and minimizing the differences between the two, using a nonlinear least squares method. This method of analysis, previously having been applied only to the more basic nightglow spectra, allows for accurate determination of temperatures and brightnesses, limited only by instrument resolution. The method also converges to the solution quite rapidly, requiring fewer calculations than a grid search or other numerical method.

Once the analysis of the spectrometer data is com$_j$'ete, a study of the effects the auroral electrons had on the upper mesosphere and lower thermosphere on that evening, was conducted. Some of these effects are time variation of vibrational band temperature and brightness, correlation of brightness and temperature variation, comparison of N I (non-ionized atomic nitrogen) emission line brightness ratios versus expected values, and vibrational population of N_2 bands.

1.3 Instrument Description

The instrument used is a Visible and Near-infrared Spectrometer (hereafter abbreviated "NIRS"), developed at the University of Michigan, and is a 1/4 meter Ebert-Fastie spectrometer (Yee *et al.*, 1991). The instrument was designed to be used on rocket flights, but was modified for

ground based operations. A brief description of the NIRS instrument and its application follows.

The NIRS optical components are illustrated in Figure 1.4, and will be described in this section. The complete cooling system and control electronics, however, will not be discussed here.

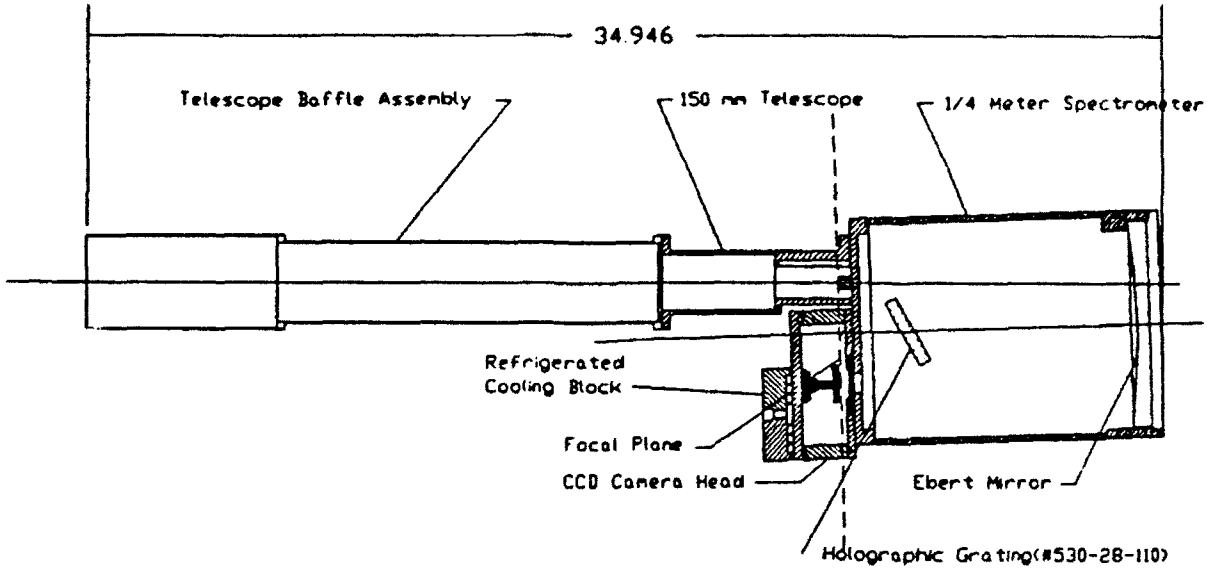

Figure 1.4 The University of Michigan Near-infrared Spectrometer.

Telescope and Baffle. NIRS observes the atmosphere through a two-stage baffled f/5 telescope. The telescope provides the light collection and pointing, and directly feeds the light collected to the spectrometer. The baffle is similar in design to the ones used in the Visible Airglow Experiment (VAE) photometers on the Atmospheric Explorers Satellites, and the Fabry-Perot Interferometer (FPI) on the Dynamic Explorer Satellites. The purpose of the baffle system is to eliminate stray light from entering the optics. Internal baffles are also installed to further minimize scattered light.

Optics. Optical parameters are listed in Table 1.1. The optical design was fully raytraced and carefully optimized to minimize the off-axis blurring due to optical aberration.

PARAMETER	SPECIFICATION
Spectral range	8355 - 8900 Å
Spectral channels	385 (1 used for dark count)
Wavelength per channel	1.3983 Å
Spectral resolution (FWHH)	12.6 Å
Telescope f -number	f/5
Objective lens focal length	150 mm
Field of view	)717 x 2.52 deg
Input slit size	0.1877 x 6.62 mm
Grating density	600 lines/mm
Interference order	1
Detector type	Thompson TH7882 CCD
Detector array size	388 x 288 pixels
Detector pixel size	23 x 23 mm
Detector temperature	−50° to −70°C
Sensitivity	1.6 el/sec/R/Å @8600 Å

Table 1.1 NIRS instrument specifications.

Ebert-Fastie Spectrometer. NIRS uses a 1/4 meter Ebert mirror and a 600 lines/mm holographic grating, and operates on the first interference

order. A blocking filter which eliminates photons with wavelength less than 6000Å is installed to prevent photons with higher order dispersion from reaching the detector.

Detector. The grating-dispersed spectrum is imaged onto a Charged-Coupled Device (CCD) detector using on-chip binning of photons. The CCD used is a MOS (metal-oxide semiconductor) optical detector composed of 111,744 (388 x 288) independent sites, or pixels, where photon-induced charge is stored. The number of charge induced is porportional to the light intensity and can accumulate over an extended period of time with its exposure length (integration time) controlled by the frequency of transfer between the storage frame and image frame. The integration time used for this study was 30 seconds.

The CCD detector system used is a modified Photometric CCD camera head with a Thompson TH7882 frame transfer CCD chip installed within it. The chip is cooled using a three stage thermo-electric cooler with flowing liquid coolant in order to decrease the thermal noise. This thermal noise exhibits itself in a CCD as dark counts (charge induced with no light entering the detector). Usually, a CCD temperature increase of a mere 7 degrees Celsius can double the thermal noise or dark counts. Thus in order to keep thermal noise well below signal levels it is important to cool the chip as much as possible. The temperature was predominantly within -65 to -75 degrees Celsius for this study.

Sensitivity. The absolute sensitivity obtained is based on an NBS (National Bureau of Standards) lamp of known spectral shape and brightness. Figure 1.5 gives the results of the calibration with 1 x 288 pixel CCD binning. As can be seen in the graph, there is somewhat less sensitivity at the end pixels or channels due to the grating slightly

overlapping the CCD chip. Approximately 0.10 digital counts/sec/R/Å (or 1.6 el/sec/R/Å) sensitivity is obtained in the spectral region near 8600Å (the analog/digital conversion factor is 15.6 electrons/digital count).

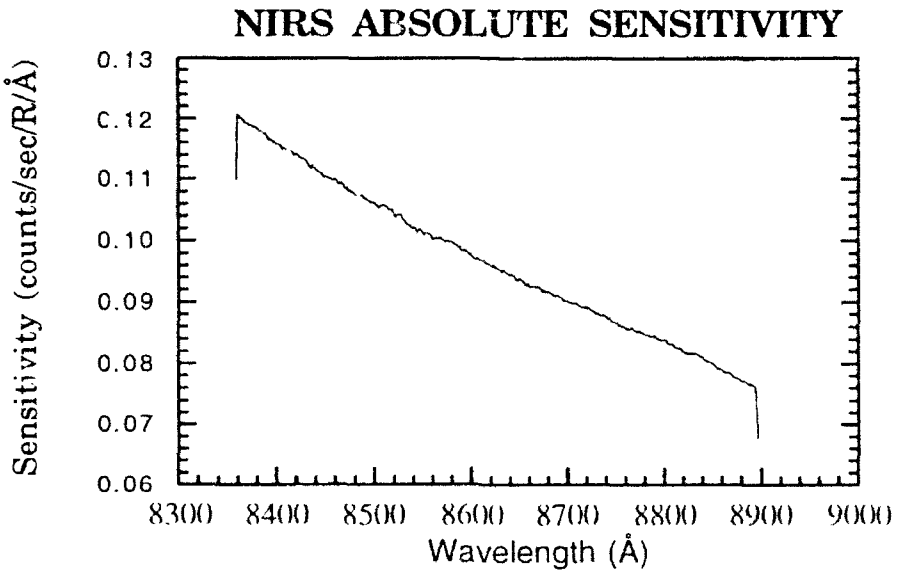

Figure 1.5 Spectrometer sensitivity for a 1 x 288 pixel CCD binning pattern calibrated January, 1991.

Resolution. The NIRS resolution can be determined from the number of pixels or channels it takes to reduce the transmission to 1/*e* of the reference pixel's transmission. With the use of Figure 1.6, it can be seen that 1/e from the peak of the instrument function is about 0.04 on the y-axis, and the number of pixels between the two points where the curve intersects 0.04 is about 9.7 Thus the 1/e resolution is 13.6 Å.

Another measure of resolution used by many researchers is the measure of full width at half height (FWHH) of the instrument function. This can also be obtained from Figure 1.6. The full width at half height for the NIRS instrument is 12.6 Å.

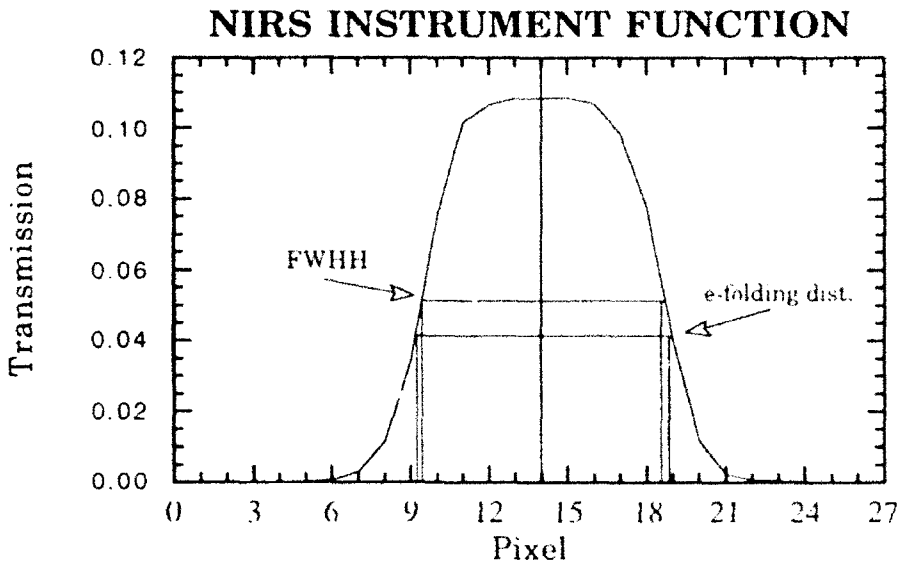

Figure 1.6 Instrument function for the spectrometer. Shows how incident radiation corresponding to channel 14 is transmitted to surrounding channels, thus affecting instrument resolution.

Chapter 2 will show how data from the instrument was analyzed and how the atomic and molecular parameters were recovered. Chapter 3 reveals results of the analysis for the atomic species emissions, and Chapter 4 gives results for the molecular species. Chapter 5 discusses conclusions drawn from this study and gives recommendations for further studies.

CHAPTER 2

ANALYTICAL METHODS

2.1 Non-linear Least Squares Method

The nonlinear least squares method is an iterative technique similar to Newton's method. It requires a first guess, though not necessarily close to the actual solution, then in each iteration it finds the fastest descent to the minimum of the function being resolved. A similar technique was demonstrated by Killeen and Hays (1984) for the analysis of Fabry-Perot interferometer data.

A remarkably few number of iterations is required for convergence to occur, and the criterion for convergence can be arbitrarily chosen by the user. In this study a value of 0.5% of each parameter was used as the convergence criterion, a fairly strict requirement. The number of iterations can be as few as 3 or 4 depending on the convergence criterion and goodness of fit. A description of the least squares method used follows.

As an introduction to notation used in the analysis, the measurement will be designated as Y, and $f(x)$ is a known function or set

of functions, called a fitting function, which we can use to predict the value of Y by varying x in an appropriate manner.

To fit more than a single parameter requires a greater number of independent simultaneous measurements, or channels, than fitting parameters, and the greater the number of channels over the number of fitting parameters the better. Thus the number of degrees of freedom is the difference, N-n, where N is the number of instrument channels, and n is the number of parameters used in the fit.

The objective is to find the fitting parameter x, by minimizing χ^2. This is done by finding the weighted difference between measurement and prediction:

$$\chi^2 = \frac{1}{N-n}\sum_{k=1}^{N}\frac{1}{\sigma_k}\{Y_k - f_k(x)\}^2, \qquad 2.1$$

where σ_k is the measurement error of the kth channel, and N and n are as defined above.

2.1.1 Solving for Parameters

Performing a first order Taylor expansion of equation 2.1, about a point a, of the function f, we get:

$$\chi^2 = \frac{1}{N-n}\sum_{k}\frac{1}{\sigma_k}\left\{Y_k - f_k(a) - \frac{df_k(a)}{dx}(x-a)\right\}^2. \qquad 2.2$$

As seen in equation 2.2, if the instrument has more than one data channel, then the measurement output Y, the output of the fitting function f, and the derivatives of f, all must be vectors, with the number of dimensions of the vectors being equal to the number of instrument channels. This also

requires some manipulation of the output of the fitting function (through the use of a convolver), so that a comparison of the fitted, synthetic spectrum, with the measurement, on a channel-by-channel basis can be accomplished. More on this will be discussed in section 2.3.

If the fitting function requires more than one variable, we need to write equation 2.2 in multi-variable form, so x and a become multi-dimensional, or vectors, and are labelled as such. Equation 2.2 now becomes:

$$\chi^2 = \frac{1}{N-n}\sum_{k=1}^{N}\frac{1}{\sigma_k}\left\{Y_k - f_k(\bar{a}) - \left[\sum_{i=1}^{n}\frac{\partial f_k(\bar{a})}{\partial x_i}(x_i - a_i)\right]\right\}^2, \qquad 2.3$$

where i varies from 1 to the number of parameters being analyzed, n, and k varies from 1 to the number of channels, N.

We can find the best possible value of each variable, x_i, which can represent species brightness or temperature for example, by minimizing the above expression. To minimize χ^2 we require the relations:

$$\frac{\partial \chi^2}{\partial x_i} = 0. \qquad 2.4$$

To simplify matters let's assume we have only two channels (N=2) and two parameters to fit (n=2). Since we need more channels than parameters, we know this would not work when trying to calculate χ^2 (because of a divide by zero error), but the system of equations can still be solved, so let's continue anyway to illustrate the mathematics. Now equation 2.3 becomes:

$$\chi^2 = \frac{1}{\sigma_1}\left\{Y_1 - f_1(\bar{a}) - \frac{\partial f_1(\bar{a})}{\partial x_1}(x_1 - a_1) - \frac{\partial f_1(\bar{a})}{\partial x_2}(x_2 - a_2)\right\}^2 + \frac{1}{\sigma_2}\left\{Y_2 - f_2(\bar{a}) - \frac{\partial f_2(\bar{a})}{\partial x_1}(x_1 - a_1) - \frac{\partial f_2(\bar{a})}{\partial x_2}(x_2 - a_2)\right\}^2 \quad 2.5$$

Using equation 2.4, neglecting third order terms, and abbreviating $f_{1,2}(\bar{a})$ as $f_{1,2}$, it can be shown that:

$$\frac{\partial \chi^2}{\partial x_1} = -2\frac{\partial f_1}{\partial x_1}\left[\frac{1}{\sigma_1}\left(Y_1 - f_1(\bar{a}) - \frac{\partial f_1}{\partial x_1}(x_1 - a_1)\right) - \frac{1}{\sigma_2}\frac{\partial f_1}{\partial x_2}(x_2 - a_2)\right] = 0 \quad 2.6$$

and:

$$\frac{\partial \chi^2}{\partial x_2} = -2\frac{\partial f_2}{\partial x_2}\left[\frac{1}{\sigma_2}\left(Y_2 - f_2(\bar{a}) - \frac{\partial f_2}{\partial x_2}(x_2 - a_2)\right) - \frac{1}{\sigma_1}\frac{\partial f_2}{\partial x_1}(x_1 - a_1)\right] = 0. \quad 2.7$$

Simplifying and rearranging equation 2.6 becomes:

$$\frac{1}{\sigma_1}\left(\frac{\partial f_1}{\partial x_1}\right)^2(x_1 - a_1) + \frac{1}{\sigma_2}\frac{\partial f_1}{\partial x_1}\frac{\partial f_1}{\partial x_2}(x_2 - a_2) = \frac{1}{\sigma_1}\frac{\partial f_1}{\partial x_1}\left[Y_1 - f_1(\bar{a})\right]$$
$$\frac{1}{\sigma_1}\frac{\partial f_2}{\partial x_1}\frac{\partial f_2}{\partial x_2}(x_1 - a_1) + \frac{1}{\sigma_2}\left(\frac{\partial f_2}{\partial x_2}\right)^2(x_2 - a_2) = \frac{1}{\sigma_2}\frac{\partial f_2}{\partial x_2}\left[Y_2 - f_2(\bar{a})\right] \quad 2.8$$

which in two-dimensional matrix form looks like:

$$\begin{bmatrix} \left(\frac{\partial f_1}{\partial x_1}\right)^2 & \frac{\partial f_1}{\partial x_1}\frac{\partial f_1}{\partial x_2} \\ \frac{\partial f_2}{\partial x_1}\frac{\partial f_2}{\partial x_2} & \left(\frac{\partial f_2}{\partial x_2}\right)^2 \end{bmatrix} \begin{bmatrix} \frac{1}{\sigma_1}(x_1 - a_1) \\ \frac{1}{\sigma_2}(x_2 - a_2) \end{bmatrix} = \begin{bmatrix} \frac{1}{\sigma_1}\frac{\partial f_1}{\partial x_1}\left(Y_1 - f_1(\bar{a})\right) \\ \frac{1}{\sigma_2}\frac{\partial f_2}{\partial x_2}\left(Y_2 - f_2(\bar{a})\right) \end{bmatrix}. \quad 2.9$$

Thus in general we get n equations and n unknowns, and we are free to choose n, the number of fitting parameters, as large as we wish, up to the number of channels on the spectrometer (the number of degrees of freedom) minus one. The matrices in 2.9 are of the form $Ax = B$ and we wish to solve for the x matrix. After doing so we can add the a_i's, which are the initial values, to arrive at the x_i's. One can use an LU decomposition or other technique to solve for the x matrix, but here we will use the simple matrix inversion method: $x = A^{-1}B$ (code adapted from Bevington, 1969), since the inverve matrix elements will come in use later on when determining the most probable errors.

This method very easily becomes an iterative method by reentering the loop, substituting the a_i's with the x_i's obtained from the previous iteration, or if it's the first iteration arbitrarily set the a_i's to some initial guess. In one line form the iteration formula may be written:

$$x_{i,m+1} = x_{i,m} + \sum_k A_{jk}^{-1} B_k \,, \qquad 2.10$$

where $x_{i,m}$is the ith parameter from the mth iteration, A_{jk}^{-1} is the inverse of matrix A, and is also a square matrix, and B has N rows and 1 column. We are now ready to test to see when the iteration can be stopped.

2.1.2 Iteration Testing

Since we have the iteration formulae, we now need to know: 1) when to stop the program from looping, and 2) how good the calculated spectra fits the measured spectra.

The first question can be answered by simply looking at the relative change of each parameter after each iteration. If the percentage change of

each parameter is less than some arbitrarily small number, then a simple "IF" statement in FORTRAN can stop the loop. In this study, if the relative change of each parameter was less than 0.5% then the loop was halted, and convergence has occurred. An exception to this rule was made for those parameters whose intensity was less than 100 R, which generally indicated a poor fitting parameter to that particular spectra.

The question of how good is the fit can be answered in part by looking at the value of χ^2. For a perfect fit, $\chi^2=1$. If the value is much greater than say 5, then the synthetic spectrum does not fit the measured spectrum well enough to say the spectrum is fully analyzed.

Now that we have the method to optimize any variable we choose, we need to know what is in the function f , which we will use in equation 2.9 to determine the A matrix which will then be inverted. The function f inputs all parameters used in the analysis and outputs a channel by channel intensity distribution for use in comparing with the instrument data.

To do this requires two basic steps: 1) take input parameters (species brightnesses and temperatures) and determine a theoretical emission spectrum, 2) take emission spectra and calculate the signal received for each wavelength interval corresponding to the NIRS instrument channels, and sum the individual intensities to get a total intensity for each channel. Step 1 requires a band model for each molecular transition being investigated, and step 2 requires a convolver which depends on individual instrument characteristics.

2.2 Band Models

As mentioned before, a band model is needed for each molecular transition being investigated. Due to the rich variety of emissions in the auroral measurements, this study required several band models. The molecular bands used to fit the aurora data are listed in Table 2.1.

Band Name	Electronic Transition	Vibrational Transitions (v',v'')	Model Author
N_2 1st Positive	$B^3\Pi_g - A^3\Sigma_u^+$	(1,0),(2,1),(3,2), (4,3)	R.L. Gattinger
O_2 Atmosperic	$b^1\Sigma_g^+ - X^3\Sigma_g^-$	(0,1),(1,2),(2,3)	P.B. Hays
OH Meinel	N/A	(6,2),(7,3)	J.H. Yee (1988)
N_2 Infrared Afterglow	$B'^3\Sigma_u^- - B^3\Pi_g$	(6,2),(11,6) (12,7)	E.J. Bucsela, T.J. Smith (1992)
N_2^+ Meinel	$A^2\Pi_{ui} - X^2\Sigma_g^+$	(4,2),(5,3)	E.J. Bucsela (1991)

Table 2.1 Molecular bands and band models used to analyzed the November 8, 1991 aurora measurements. The OH Meinel bands are due to pure vibration-rotation transitions, so an electronic transition is not applicable for this case.

The basic principle of each of the above models is the same: input the desired vibrational transition, temperature, and band brightness, and the model outputs an array of emission line wavelengths and an array of associated line strengths. The number of lines output is on the order of hundreds to over a thousand for each band. An example of output from a band model is given in Figure 2.1. Figure 2.2, shown next to Figure 2.1 for comparison purposes, is what Figure 2.1 looks like once the lines are

convolved, i.e., binned by wavelength and converted to a "measurement" as seen by the spectrometer. The convolver subroutine is discussed in the next section.

Once all the appropriate models have been called in the computer program, the arrays of wavelengths and strengths are stacked so that you are left with one array of wavelengths and one array of line strengths. These arrays are next fed into the convolver subroutine.

2.3 NIRS Convolver

The NIRS Convolver subroutine was written by J.H. Yee for use in determining atomic emission intensities and molecular emission temperatures and intensities from the instrument data. I will merely describe the principles used to write the subroutine.

The idea of the convolver subroutine is simple: take the arrays of line wavelengths and associated line strengths, compute the signals according to the instrument function and sensitivity profiles shown in Figures 1.3 and 1.4, then add up the signals within wavelength bins which correspond to instrument channels. This procedure takes thousands of individual lines and converts them to a 384 channel predicted measurement which can then be used to compare with the actual data. An example of a convolved molecular band was shown in fig. 2.2.

It should now be evident that the function f sought in section 2.1 is simply a summation of all lines, molecular band lines and atomic lines, convolved into a 384 channel prediction. Thus we can build a subroutine which calls the desired band model subroutines with input band temperatures and intensities, then convolves the many lines into a useful

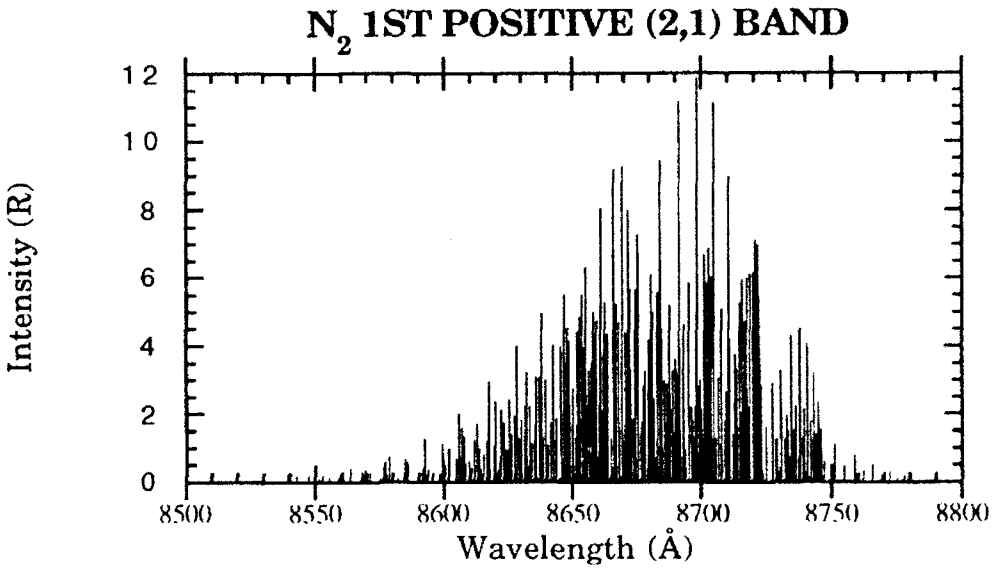

Figure 2.1 An example of band model output - N2 first positive (2,1) band at 1000 R band intensity and 300 K.

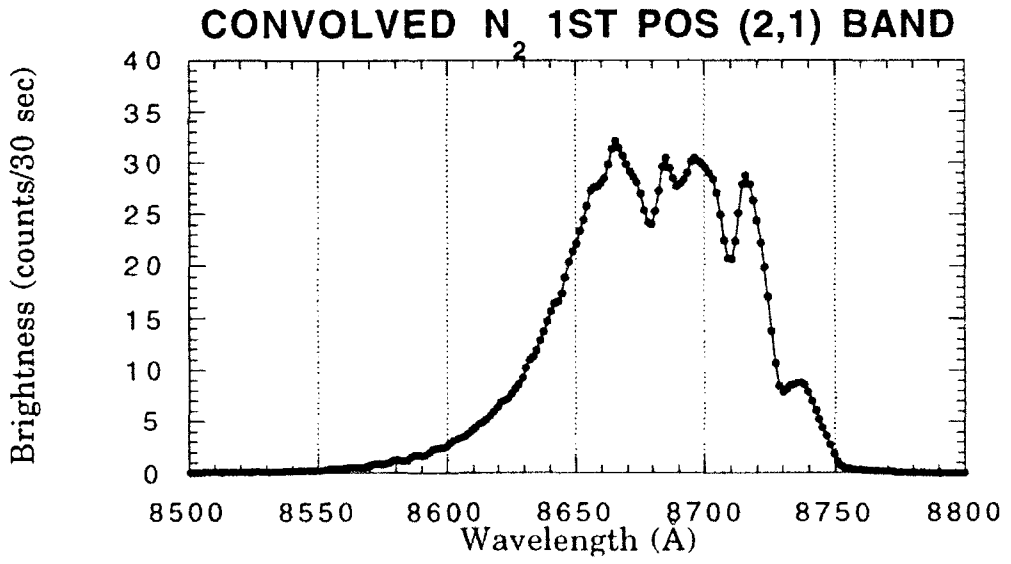

Figure 2.2 Convolved N2 1st positive (2,1) band at 1000 R band intensity and 300 K.

form. This subroutine is like the function f, used earlier in this chapter, which we can use to find the $f(a)$ or $\frac{df}{dx_i}$ arrays in equation 2.9.

2.4 Error Analysis

When measuring the aurora with a CCD spectrometer, there are three basic types of noise which must be dealt with in some way: 1) thermal noise (dark counts), 2) instrument bias (read noise), and 3) photon statistics. The treatment of each of these will be discussed separately.

2.4.1 Thermal Noise

A CCD detector produces thermal noise or dark counts which is greatly dependent on temperature. As mentioned previously the detector system used for this study incorporated a 385 channel CCD binning pattern, with 384 columns of pixels used as data channels, and 4 columns of pixels used to measure dark counts.

The dark count columns of pixels were covered so that no external radiation would be detected at these columns of sites, which were used as a single channel. It is assumed that any counts detected from this channel must be due to thermal noise which is dependent on the CCD temperature, assumed to be uniform across the chip. Using these assumptions the thermal noise can be calculated and carefully removed, as much as possible, by simply subtracting the number of dark counts detected by the 385th channel from each of the other 384 channels. One way to do this is by using an approximation for the CCD temperature from the dark count measurement:

$$T_{CCD}(^{\circ}C) = -50 - H_{385} \ln(\frac{C_{385}}{C1_{385}} \Delta t), \qquad 2.11$$

where H and $C1$ are simply coefficients for the $385th$ channel (the dark channel) as measured during calibration, C is the number of dark counts measured during the 30 second integration period (Δt), and -50 degrees was chosen arbitrarily as a reference temperature. To subtract the number of dark counts from the ith channel measurement, we use the relation:

$$c_i = c_{i0} - \Delta t \cdot C1_i \exp(\frac{T_{CCD} + 50}{H_i}), \qquad 2.12$$

where c_{i0} is the original measurement of the ith channel, and c_i is now the measurement adjusted for thermal noise. It is agreed there are a few redundant calculations in the above equations, but these equations were chosen for ease of understanding, versus ease for computation.

2.4.2 Instrument Bias (Read Noise)

This noise is introduced by the readout amplifier of the CCD electronics. For each read that occurs, a slight error in the number of counts read is introduced. The magnitude of the error introduced is on the order of 1 count/read, where a read must be accomplished to retrieve data from each channel, for each frame of data. The instrument bias is corrected for by simply taking the bias (determined from laboratory calibration) and subtracting it from the measurement of each channel.

2.4.3 Photon Statistics

This type of noise cannot be corrected for as with the above types of errors because we are uncertain of the amount of the error involved in each

measurement within known bounds. However, statistical errors usually follow a Poisson distribution:

$$\Delta I = \frac{\sqrt{I}}{I}, \qquad 2.13$$

where I is the measured signal, expressed in units of number of electrons.

From this relation we can see that the greater the signal, the smaller the relative error. To exploit this all we need to do is increase the instrument's integration time, or time the shutter remains open, to increase intensity, thereby lowering relative error.

As an example of how this integration helps, let's compare the relative error of low and high intensity measurements at 1 versus 30 second integration time. During the early evening hours (when the aurora was active) the spectrometer recorded counts between 10 and 100 counts per second. Once the aurora quieted down, after 9 PM, nightglow emissions predominated and only about 1-10 counts per second were recorded.

Table 2.2 shows a comparison of the statistical errors calculated from equation 2.13, remembering the error is based on electron counts not digital counts. Thus, the I in equation 2.13 is the number of digital counts measured, multiplied by 15.6 electrons/digital counts, which is then substituted into the equation for error determination. As an added note, throughout the remainder of this writing, "counts" will refer to digital counts, not number of electrons. Conversion to number of electrons is necessary when figuring photon statistics.

As can be seen from the table, a 30 second integration period decreases statistical error by a factor of about 5! Of course this increase in accuracy is not free. Since we are integrating over 30 seconds we are losing

that much temporal resolution, but not enough to be deemed important. A 30 second resolution is sufficient for most any study.

Also seen from Table 2.2 is the fact that measurements taken during the auroral maximum period, 30 second integration time, are accurate to within 0.5% (for peak intensity channels) to 2.5% (for least intense channels). However, between 9-12 PM, measurements are accurate only to within 1.5% to 8.0%.

Measurement Condition	**Intensity** (counts/sec)	**Relative Error**	
		1 sec int per	**30 sec** int per
Low int. nightglow	1	25%	4.6%
High int. nightglow, Low int. aurora	10	8.0%	1.5%
High int. aurora	100	2.5%	0.5%

Table 2.2 Comparison of statistical error of measurements with 1 second versus 30 second integration period under different brightness conditions.

An estimate of statistical error of a particular fitting parameter can be obtained quite simply. The uncertainty in fitting the j th parameter, a_j, is given by:

$$\sigma_{a_j} = \sqrt{\varepsilon_{jj}}, \qquad 2.14$$

where ε_{jj} is the j th diagonal element of the error matrix, ε. The error matrix is basically the inverse matrix, A^{-1}, for which we have already

solved to recover the a_j's. The σ's, then, are the analytical errors of the fitting parameters.

2.4.4 Systematic Error

The predominant type of systematic error in the spectrometer measurements occurs because of absolute sensitivity. The sensitivity calibrations are accomplished using a known continuum source, with its brightness traceable to an NBS lamp, as described in chapter 1. Calibrating an instrument to this lamp does not guarantee absolute accuracy. In fact, the NIRS instrument can only claim an accuracy of 15% due to the uncertainty of the standard.

Other types of systematic error arise because of imprecise methods used in various stages of the fitting function. Some examples are assumption of only electric dipole transitions in band models, imprecise molecular constants used to calculate band model output, assumption of thermal equilibrium among rotational levels, etc.

2.5 Preliminary Results

An analysis of the spectrometer data was done in the manner described in previous sections. Table 2.3 lists the parameters used in the non-linear least squares technique to create a synthetic best-fit spectrum. The table of parameters is just one of nearly 600 frames analyzed and represents typical intensities and temperatures recovered during the period of higher auroral activity.

On page 31, Figure 2.3 shows how those parameters fit the spectrum. A two-parameter continuum was used to allow for better fitting of the data since it is presumed that the background radiation is not a constant across the spectrum. At least 10 atomic oxygen and nitrogen lines were found to exist in the spectrum and 14 molecular bands were analyzed as well. A detailed description of the analysis of atomic species is given in chapter 3, and the description of the molecular species analysis is given in chapter 4.

	Parameter	Value	Units	Error*
1	Hi l continuum	8.51	R	1.69
2	Lo l continuum	25 87	R	0.63
3	O I 8446.5 Å	8548.51	R	18.05
4	N I 8567.7 Å	123.75	R	8.01
5	" 8594.0	434.60	R	11.10
6	" 8629.2	1131.00	R	24.05
7	" 8655.9	521.50	R	19.79
8	" 8680.3	4869.28	R	34.42
9	" 8683.4	5627.37	R	35.83
10	" 8703.3	804.16	R	37.43
11	" 8711.7	1164.04	R	23.67
12	" 8718.8	707.81	R	33.89
13	N_2 1P (1,0)	32834.50	R	273.45
14	" (2,1)	24009.21	R	334.62
15	" (3,2)	3401.74	R	80.47
16	" (4,3)	490.62	R	500.01
17	" temp	383.05	K	4.08
18	O_2 Atm (0,1)	11115.95	R	97.33
19	" temp	432.07	K	3.17
20	O_2 Atm (1,2)	4559.97	R	162.90
21	" (2,3)	1356.45	R	64.53
22	" temp	637.69	K	16.17
23	OH (6,2)	1703.79	R	58.68
24	" (7,3)	2501.85	R	110.30
25	" temp	158.84	K	3.70
26	N_2 IRA (11,6)	4103.61	R	150.08
27	" (6,2)	1438.56	R	114.62
28	" (12,7)	5919.23	R	439.84
29	" temp	640.40	K	30.44
30	N_2^+ (4,2)	3186.54	R	141.76
31	" (5,3)	1589.56	R	196.00
Time: 19.0167		χ^2 = 21.67		

Table 2.3 List of the 31 parameters used in this study to analyze a typical measurement spectrum, with an integration period of 30 seconds. (* Note that since the value of Chi-squared is not equal to 1 the error values in the above table are not representative of the true analytical uncertainty).

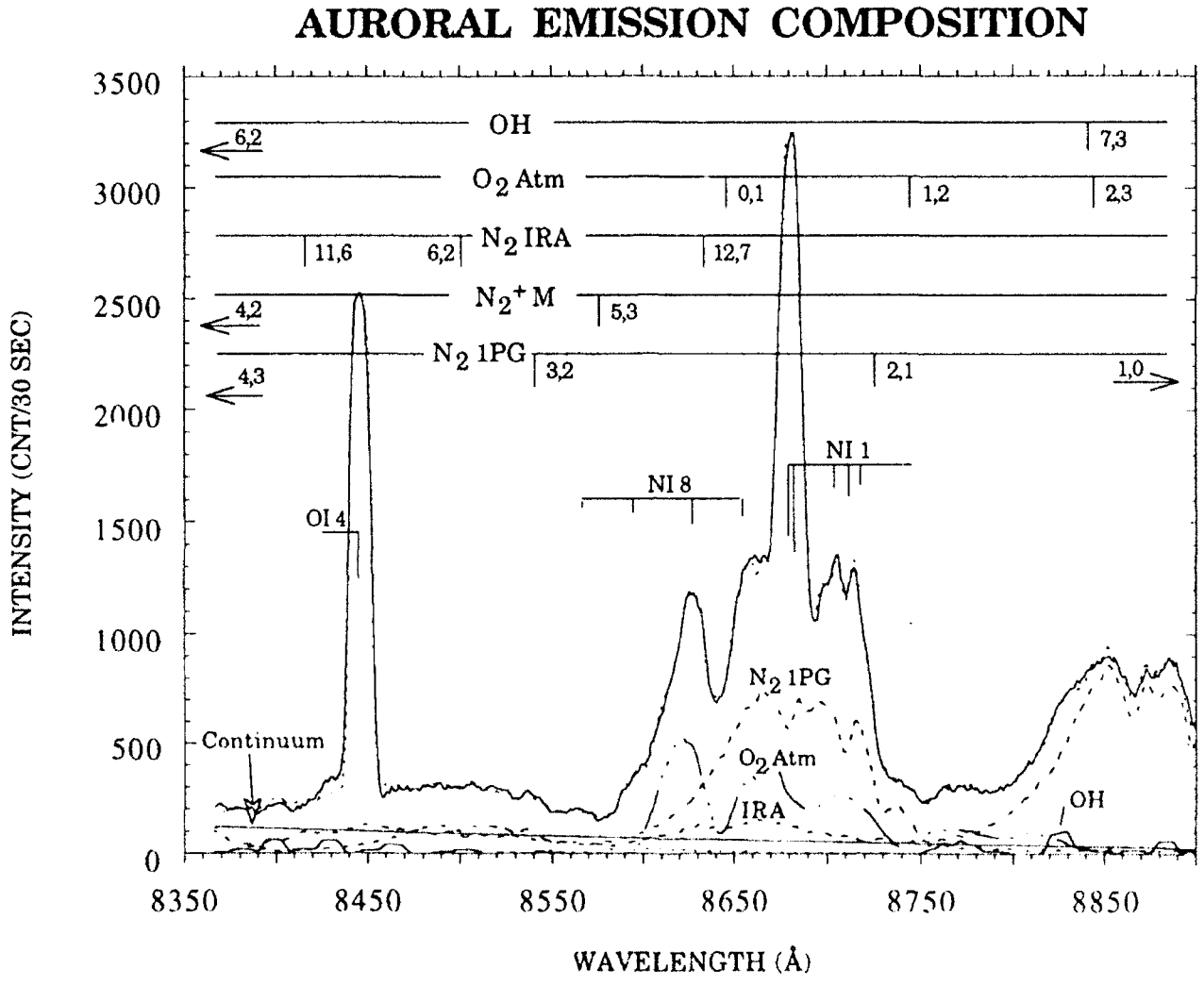

Figure 2.3 Total analyzed composition of the November 8, 1991 aurora over Ann Arbor, MI. The top solid line indicates the measurement, dotted indicates fitted spectrum, lower lines indicate fitted molecular parameters and continua.

CHAPTER 3

ATOMIC EMISSIONS

3.1 Atomic Structure

Before the features of atomic emissions can be discussed, atomic structure must first be understood. I will not go into great detail of the structure, but enough to provide a background so that an understanding of the discussion that follows is possible. This section, as well as a much more detailed discussion can be found in Herzberg (1945).

The Schroedinger equation, which describes the motion of the electrons in an atom, requires at least four quantum numbers to uniquely define the state of a particular atomic electron:

n: principle quantum number

l: orbital quantum number

m_l: orbital magnetic quantum number

m_s: spin magnetic quantum number.

According to the Pauli Exclusion Principle, no two electrons can have the same set of four quantum numbers in an atom or molecule.

The principle quantum number, n, is related to the probability of finding the electron a certain distance from the nucleus. For historical reasons, all electons with the same principle quantum number are said to be in the same electonic shell, identified by the letters: K,L,M,N,O, or P for n=1,2,3,4,5, or 6, respectively. Likewise electrons having the same value of both n and l quantum numbers are said to be in the same subshell, designated as: s,p,d,f,g, or h when l=0,1,2,3,4, or 5 respectively.

As an example of notation, the ground (or valence) electronic configuration of atomic oxygen is: $1s^2 2s^2 2p^4$. This means there are 2 electrons in the 1s subshell (or K shell, n=1). Likewise the 2s subshell has 2 electrons, and 2p has 4 electrons. The four quantum numbers are related as given in Table 3.1.

Quantum Number	# Possible Values	Range of Values
n	1	
l	n	0,1,2,...,n-1
m_l	2l+1	-l,-l+1,...,l
m_s	2	-1/2, 1/2

Table 3.1 Relationship of the four atomic quantum numbers.

The presence of an external magnetic field gives rise to splitting in spectral lines, because of the field's interaction with the spin of the electron (anomalous Zeeman Effect). This splitting can be very small or quite measureable. An example of this can be seen in Table 3.2. The splitting of

the three OI lines is on the order of 0.1Å, but for the NI 8 series, the splitting is on the order of 10's of Angstroms.

To arrive at energy states of an atom we must add the respective angular momenta of the individual electrons. The energy state, or term type, of an atom is written in the general form:

$$^{2S+1}L_J, \tag{3.1}$$

where L is the resultant angular momentum quantum number, S is the resultant spin quantum number, and J is the resultant total angular momentum quantum number, and can take on values from $J = |L+S|,\ldots,|L-S|$. When L=0,1,2, or 3 for an atom, the state is denoted as a/an S,P,D, or F state (analagous to the electron shell designation).

The ground state of atomic oxygen, $1s^2 2s^2 2p^4$, has term type:

$$^3P_{2,1,0}. \tag{3.2}$$

From this notation we know that L=1 (P), S=1 (2S+1=3), and since in general, a state with a left superscript of three denotes a triplet, or energy state split into three states, J can take on a value of either 2, 1, or 0. The exception to the rule, that the superscript equals the number of split levels, occurs when the resultant quantum number, L, is less than the resultant quantum number S. In that case the number of split levels is equal to L. We can now go into specifics of atomic oxygen and nitrogen emissions and what causes them.

3.2 Atomic Lines in the Aurora

There are a number of atomic lines in the 8400-8900Å spectral region which must be included in any analysis of auroral emissions. The atoms that need to be considered are primarily those of the O and N atoms, since these atoms are some of the most abundant in the altitude region of the aurora, 100-200 km. A more complete analysis would need to include emissions from N^+ as well. The ionic species were neglected for this study because it was attempted to keep the number of parameters to a minimum, and their emission intensities were expected to be small.

3.2.1 Production Mechanisms

The production of the excited states of the O and N atoms responsible for the emissions may be due to inelastic collisions of the form,

$$e + X \rightarrow X^* + e, \tag{3.3}$$

or the result of atom-atom or molecule-atom energy transfer,

$$M^* + X \rightarrow M + X^*, \tag{3.4}$$

where X may be either an N or O atom, M may be any atom or molecule, and an asterisk denotes an excited species (Jursa, 1985). Another possibly equal production mechanism for excited N, suggested by Fillipini, et al. (1982), is:

$$\begin{aligned} N_2 + e &\rightarrow N_2^{+*} + 2e \\ N_2^{+*} &\rightarrow N^+ + N \end{aligned} \tag{3.5}$$

Once the excited species of O or N is created, a radiative transition may occur, and the speed of transition, or the inverse of radiative lifetime, is determined by selection rules of the transition. For a detailed discussion of selection rules and types of transitions, again see Herzberg's book. Magnetic dipole and electric quadrupole transitions occur considerably slower than electric dipole transitions. Typical radiative lifetimes for the N species electric dipole allowed emissions are 10^{-8} seconds- very fast.

3.2.2 Emission Lines

A list of all known OI (neutral O), OII (O^+), NI, and NII atomic lines in the 8400-8900Å spectral region is given in Table 3.2. The numbers in italics indicate lines used in this study, and the three 8446Å OI lines were combined as discussed in the next section. A brief discussion of each atom's excited state(s) as well as findings in the auroral analysis are given in sections 3.3 and 3.4.

The O and N lines selected from table used to analyze the aurora spectra, are primarily the strongest lines, indicated by the relative intensity in Table 3.2. The less intense lines (those less than 500 relative intensity) and ionic species were omitted to minimize parameters involved.

	Wavelength (Å)	Origin	Relative Intensity	Einstein Probability A ($10^8 sec^{-1}$)
1	8426.16	OI	120	
2	8438.74	NII	550	
3	8446.25	OI	810	
4	8446.36	"	1000	
5	8446.76	"	935	
6	8567.74	NI 8	500	0.0458
7	8594.00	"	570	0.190
8	8629.24	"	650	0.238
9	8655.89	"	500	0.099
10	8676.08	NII	220	
11	8680.28	NI 1	700	0.191
12	8683.40	"	650	0.133
13	8686.15	"	500	0.079
14	8687.43	NII	110	
15	8699.00	"	110	
16	8703.25	NI 1	500	0.171
17	8710.54	NII	160	
18	8711.70	NI 1	570	0.101
19	8718.83	"	500	0.054
20	8820.43	OI	325	
21	8728.89	NI 1	250	0.030
22	8747.36	"	200	0.0079

Table 3.2 Known oxygen and nitrogen atomic emission lines from 8350-8900Å. Numbers in italics indicate atomic lines used in this study. (Wavelengths and relative intensities from Weast, 1988; transition probabilities from Wiese et al., 1966).

3.3 Atomic Oxygen

3.3.1 Source of Emission

The ground (valence) state electronic configuration of the O atom is $1s^2 2s^2 2p^4$. As seen from Figure 3.1, the source of the OI (neutral oxygen) 8446.5Å emission line is the transition between Rydberg states

$(1s^2 2s^2 2p^3)3p\ ^3\mathrm{P}$ to $3s\ ^3S^o$. Since the upper state (^3P) is a triplet multiplet, and the lower state is a singlet multiplet, there are actually three emission lines with slightly different wavelengths coming from this transition: 8446.25, 8446.36, and 8446.76Å, with relative strengths of 810,1000, and 935 respectively (Weast, 1988).

3.3.2 Analysis

Since the instrument has a FWHH resolution of 12.6Å (from section 1.3.1), it is not able to distinguish any of the three OI 8446 lines discussed in the above section apart from one another, and we cannot determine the relative intensities of the three individual lines. Instead, a single line at 8446.5Å was used, and the intensity of this line was obtained from the least squares technique discussed in section 2.1.

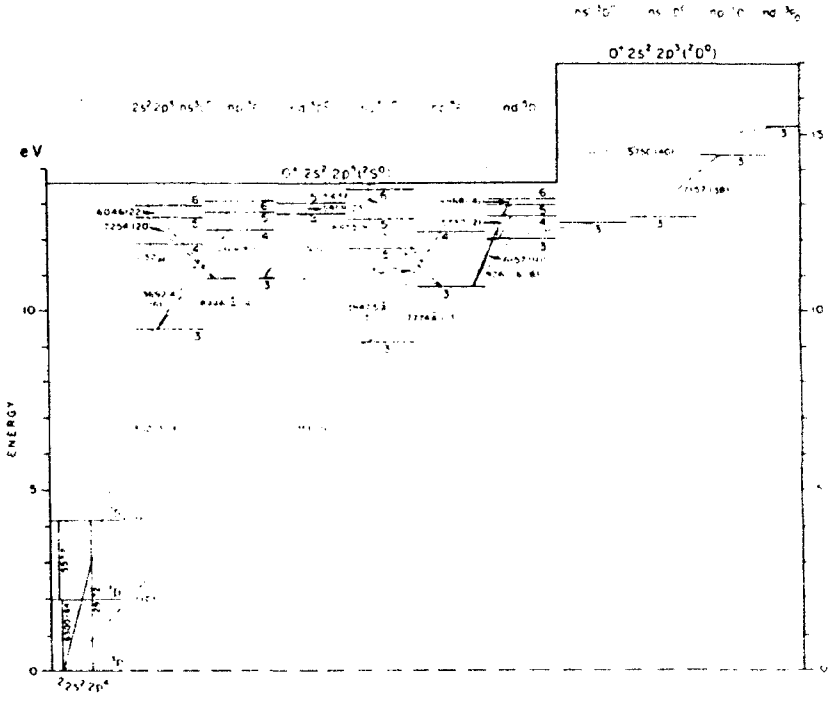

Figure 3.1 Energy level diagram of the O atom. Solid lines correspond to lines observed in aurora; the dashed lines indicate doubtful or predicted emissions. The numbers in brackets are multiplet numbers from Moore (1945). (from Vallance Jones, 1974).

Figure 3.2 shows how the intensity of the OI 8446 line varied with time from 18.5 up to 21.3 EST, when the aurora all but ended over Ann Arbor, Michigan.

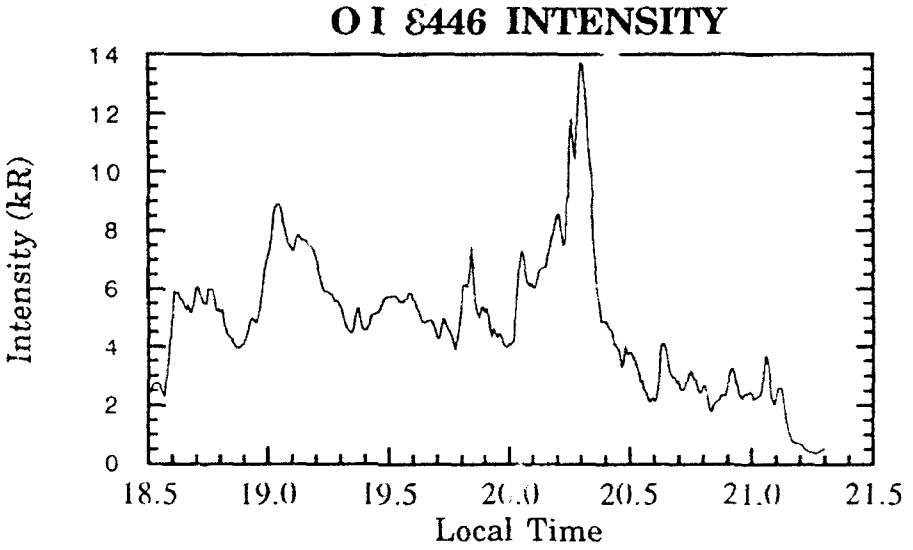

Figure 3.2 Intensity of the OI 8446Å line versus time (EST).

As can be seen from the graph, the 8446 line intensity varies quite rapidly and appears to be very sensitive to energetic particle flux. From figure 3.1 we know that the O atom needs at least 11 eV of energy gained from collisional processes of equation 3.1 or 3.2. From equation 3.1, the electrons in the 11 eV energy range are secondary electrons, which were created from other more energetic secondary electrons or primary electrons. One possible candidate for a particle of the type in equation 3.2 is energetic O or O^+ created from the aurora's influx of energetic electrons.

3.4 Nitrogen

3.4.1 Source of Emission

The number of atomic nitrogen lines is much greater than that of atomic oxygen in the range of 8400 - 8900 Å. This is simply due to energy states of the N atom being in the right place and of the right separation to be present and distinct from each other in this spectral region. Figure 3.3 shows the two transitions responsible for the NI 1 and 8 series of emission lines.

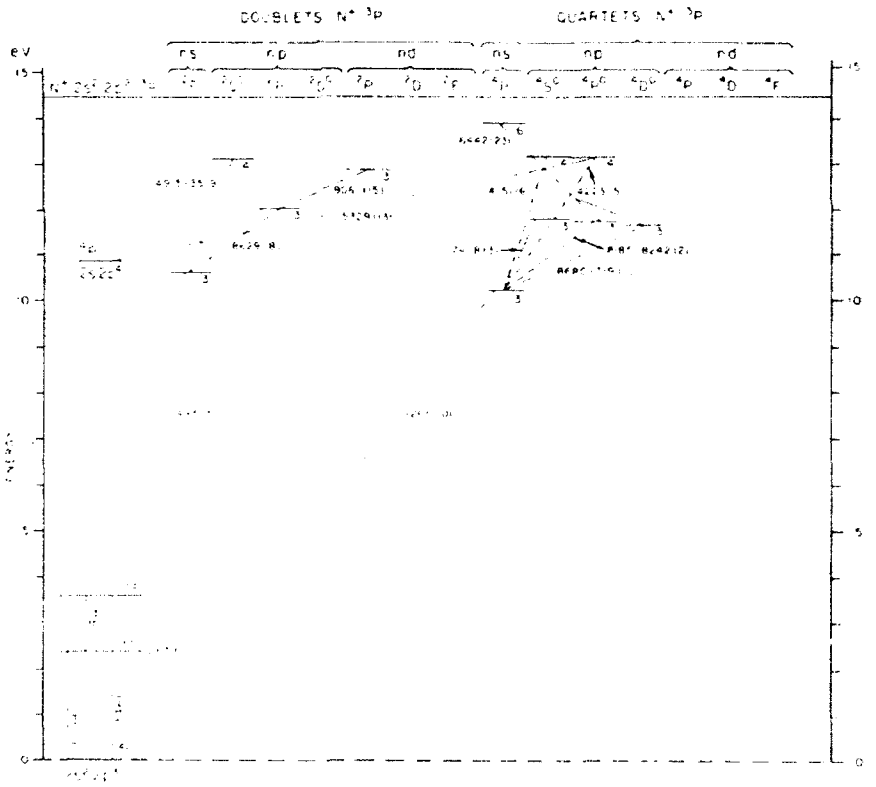

Figure 3.3 Energy level diagram of N atom, illustrated the same as Figure 3.1. (from Vallance Jones, 1974).

For the NI 1 series, the transitions take place from $(1s^2 2s^2 2p^3)3p\ ^4D^\circ$ to $3s\ ^4P$, giving a total of 8 allowed transitions or emission lines. In the case of NI 8, the transition is from $3p\ ^2P^\circ$ to $3s\ ^2P$, yielding 4 allowed transitions or emission lines. Table 3.1 gives a listing of each wavelength and Einstein transition probability for the NI 1 and NI 8 series of emission lines. Notice only the strongest lines (the ones with the highest Einstein probability) in the NI 1 series were used in this study for simplicity sake. It was also felt that the weakest lines would not overcome statistical errors to be analyzed in a consistent manner. Again, ionic emissions were not analyzed.

3.4.2 Analysis

A time plot of each of the nine atomic nitrogen emission lines is shown in Figures 3.4 and 3.5. It is immediately obvious that all of the lines follow the same general time pattern. The only exception is where the NI 1 8680 and 8683 lines change possession of the lead near 18.9 EST in Figure 3.4. It is not clear if this is an anomaly of the analysis of the data or if it is indeed truth.

As a test of how reasonable the analyzed line intensities are, we can determine the ratio of two lines, and compare the ratio with some experimental results. To do this we can use the relation:

$$\frac{I_1}{I_2} = \frac{\eta_1}{\eta_2} = \frac{N_1}{N_2}\frac{A_1}{A_2}, \qquad 3.6$$

where η is volume emission rate, and N is the total number density of the upper state.

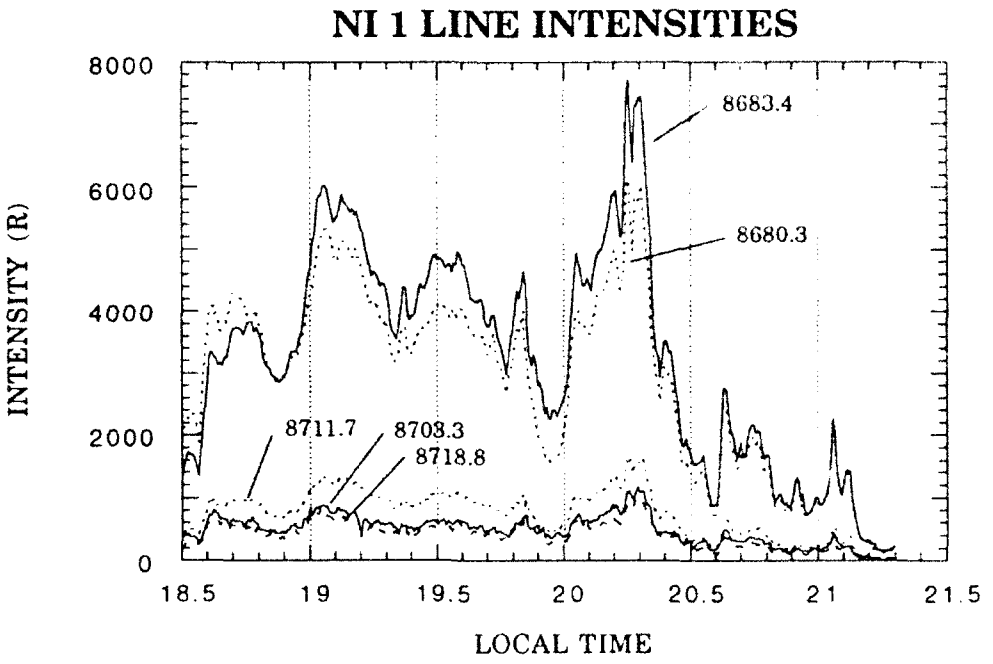

Figure 3.4 Time series of the analyzed NI 1 emission lines.

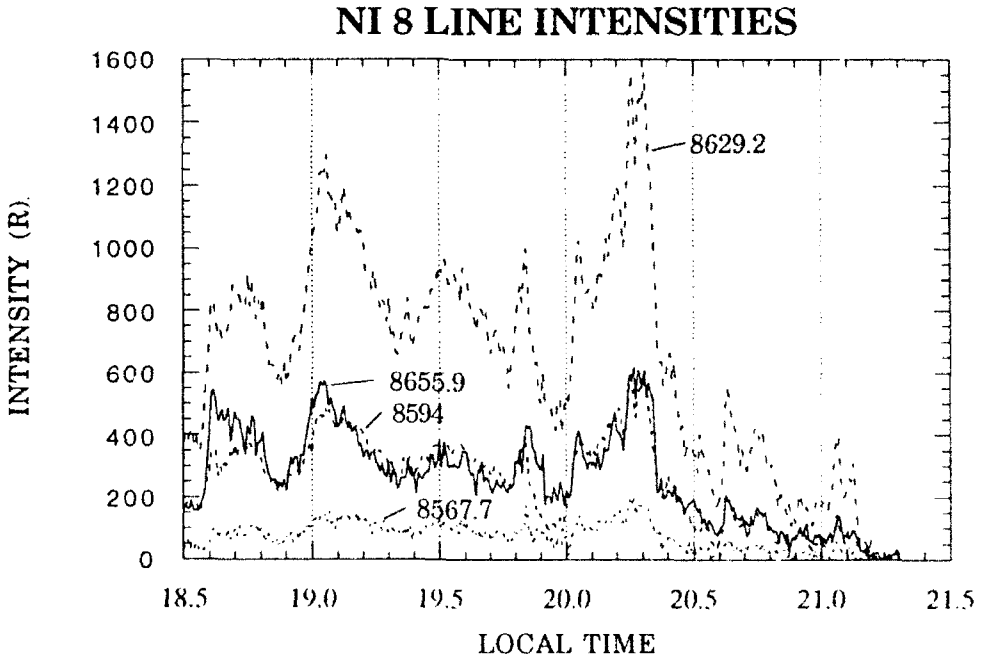

Figure 3.5 Time series of the analyzed NI 8 emission lines.

If the two emissions to be compared are from the same upper state, then $N_1 = N_2$, so we can simplify equation 3.6 to:

$$\frac{I_1}{I_2} = \frac{A_1}{A_2}, \qquad 3.7$$

which is just the ratio of the Einstein transition probabilities, and we do not need to work with number densities at all. For comparison purposes, two emission lines were chosen from each series, NI 1 and NI 8. Using the Einstein probabilities from Table 3.1, a comparison has been made of the ratios from the two sets of lines, to the expected values obtained from the transition probabilities. Figures 3.6 and 3.7 show the results.

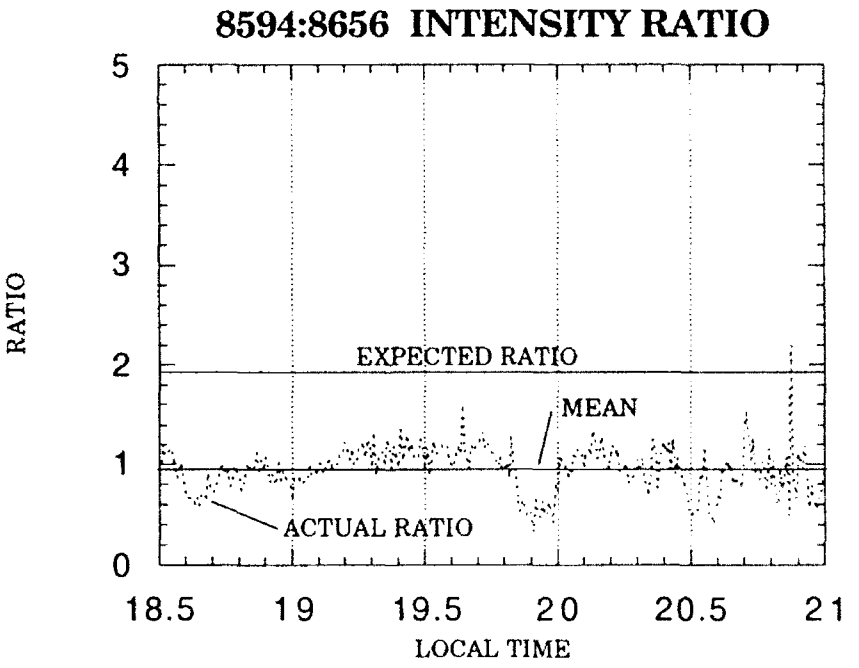

Figure 3.6 Intensity ratio of the 8594.0Å to 8655.9Å lines of the atomic nitrogen NI 8 series.

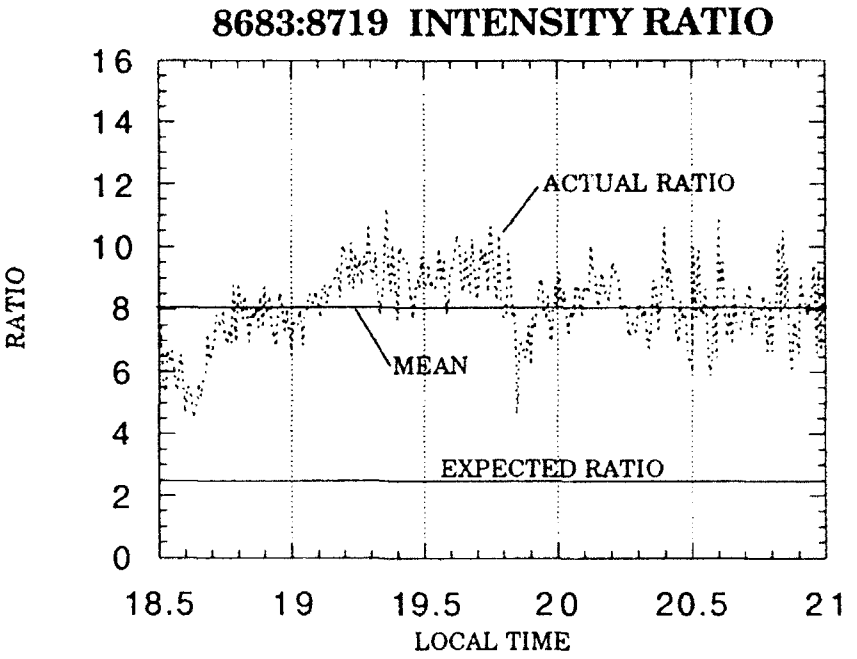

Figure 3.7 Intensity ratio of the 8683.4Å to 8718.8Å lines of the atomic nitrogen NI 1 series.

As can be seen from Figures 3.6 and 3.7, there is not ideal agreement between the analyzed data and the experimental data, taken from Wiese et al. The analyzed line ratio is off by a factor of 1/2 in Figure 3.6 and a factor of about 3.5 in Figure 3.7. If the transition probabilities are indeed accurate, a probable explaination for these deviations is that the synthetic spectrum is incompletely analyzed, resulting in improper relative intensities. This may be partially attributed to the unexpectedly large continuum values discussed in more detail in chapters 4 and 5.

CHAPTER 4

MOLECULAR EMISSIONS

4.1 Background

4.1.1 Molecular Term Type Notation

Molecular term type notation is very similar to the atomic case discussed in chapter 3. Both cases are shown here for comparison purposes:

Atom	Molecule
${}^{2S+1}L_J$	${}^{2S+1}\Lambda_\Omega$

The primary difference is where S,P,D,F are used when the resultant angular momentum number, L=0,1,2,3 for atoms, molecular notation uses Σ,Π,Δ,Φ when L=0,1,2,3. Just as for atoms, S is the resultant spin quantum number, and Ω (instead of J) is the resultant total angular momentum quantum number for molecules. Using the example in chapter 3 to show the similarity, the ${}^3P_{2,1,0}$ would be, in the molecular case, ${}^3\Pi_{2,1,0}$.

4.1.2 Emission Analysis

An advantage of analyzing the spectra for molecular emissions is that one can recover temperatures from the rotational distribution of each vibration-rotation band analyzed without a high resolution instrument. This requires of course a band model for the particular type of transition involoved, as mentioned in chapter 2.

The molecular emissions analyzed in this study, in order of intensity of emission, are: N_2 1st Positive (N_2 1PG), O_2 Atmospheric (O_2 Atm), N_2 Infrared Afterglow (N_2 IRA), N_2^+ Meinel (N_2^+ M), and hydroxyl (OH). The best fit obtained from the 31 parameters listed in Table 2.3 is shown in figure 4.1.

In Figure 4.1, the highest solid line is the corrected measurement at time 19.02 (19:01 EST), the dotted line near the measurement line is the total fitted synthetic spectrum with all 31 parameters' contributions added together, though only the molecular contributions are shown in the graph, located below the data and fitted lines. The atomic species were discussed in chapter 3.

At the top of the graph are the band origins of the vibrational transitions of each species analyzed. As an example of what the notation means, the bottom line shows where the N_2 1PG (2,1) band origin is located. The "2,1" means the transition takes place from rotational levels of vibrational level 2 of the upper electronic state, to rotational levels of vibrational level 1 of the lower electronic state. An arrow in Figure 4.1 indicates band origins which are outside the range of the data but still have tails which contribute to the overall spectrum. Figure 4.2 is an illustration of all three types of energy levels in a molecule: electronic, vibrational, and rotational.

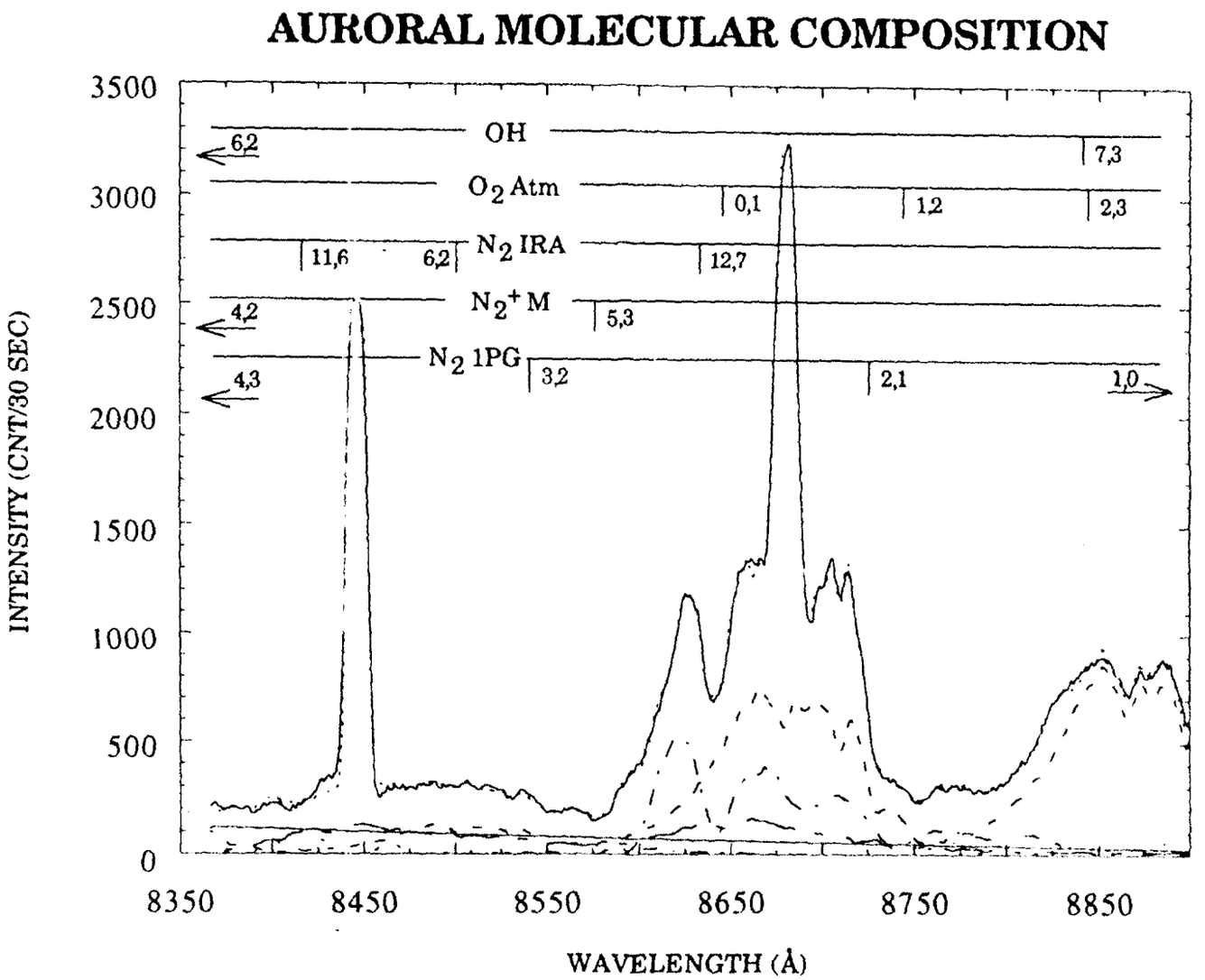

Figure 4.1 Analyzed molecular composition of the November 8, 1991 aurora over Ann Arbor, MI. The top solid line indicates the measurement, dotted indicates fitted spectrum, lower lines indicate fitted molecular parameters and continua.

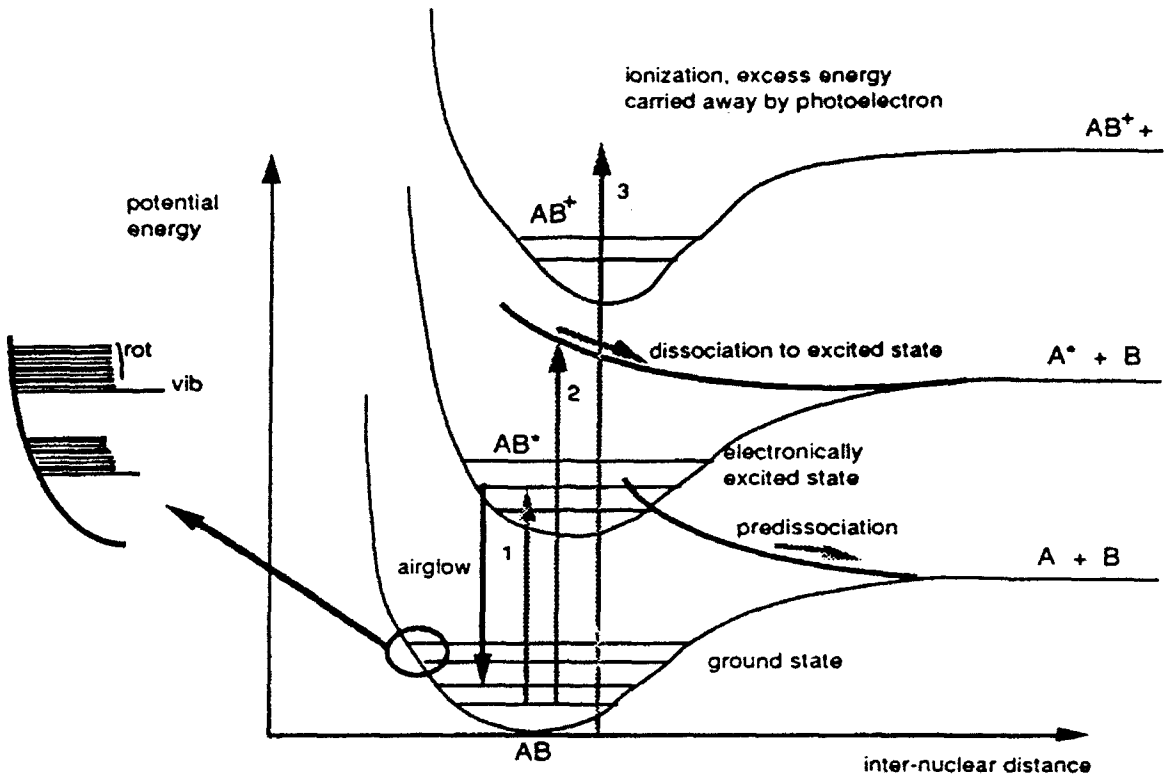

Figure 4.2 Energy level of a typical molecule showing electronic, vibrational, and rotational energy levels.

The solid line near the bottom of the graph is the continuum used to fit the spectrum's "leftovers". As seen in Table 1.2 the continuum varied from 25.87 R/Å at 8400Å down to 8.51 R/Å at 8900Å. The 25.87 R/Å continuum parameter is a much higher value than expected. Much effort was spent trying to lower this parameter. More on the continuum will be discussed in chapter 5.

4.2 Nitrogen

Diatomic nitrogen accounts for a major portion of auroral emissions. Figure 4.3 shows the electronic energy states of N_2. Two separate N_2, and one N_2^+, band systems were analyzed in the 8400-8900Å spectrum: 1) the first positive system, which occurs due to $B^3\Pi_g - A^3\Sigma_u^+$ transitions of N_2 as can be seen in Figure 4.3, 2) the infrared afterglow system (IRA), occurring due to $B'^3\Sigma_u^- - B^3\Pi_g$ transitions, and 3) the N_2^+ Meinel system, from $A^2\Pi_{iu} - X^2\Sigma_g^+$ transitions. Each system will be covered separately.

4.2.1 First Positive System

This system represents the most intense and dominant feature in the spectrum considered. The production of the B-state is produced from energetic electron collisional excitation either directly from the X-state (the ground state) or indirectly through the C or B' states, for example, cascading down to the B-state through radiative processes. The $B^3\Pi_g - A^3\Sigma_u^+$ transition is a spin-allowed electric dipole transition and occurs very fast: the radiative lifetime of the B-state is on the order of 10^{-5} seconds (Loftus and Krupenie, 1977), and the primary means of deexcitation is through the first positive radiative process.

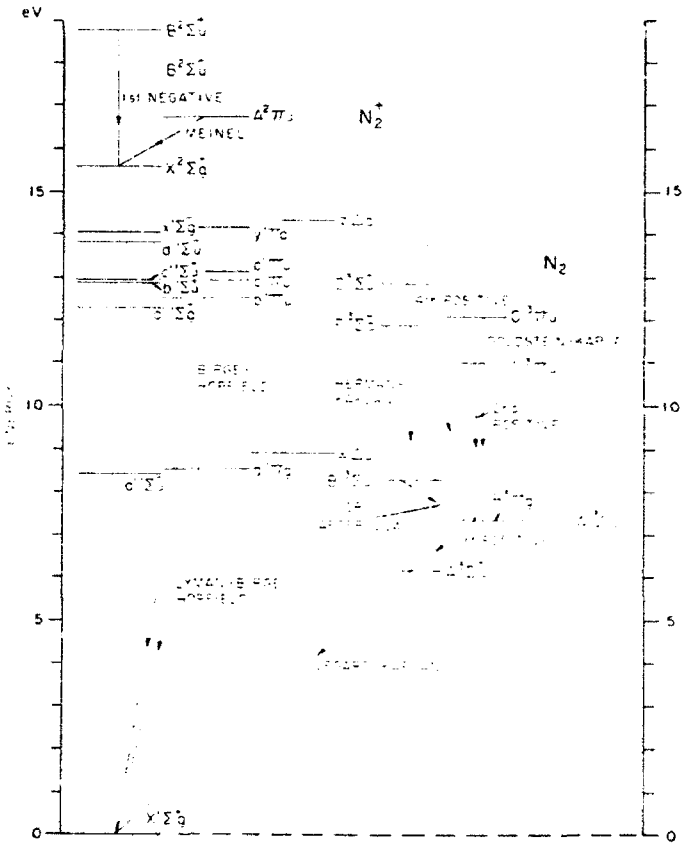

Figure 4.3 Potential energy levels and electronic band systems for N_2 and N_2^+ illustrated the same as Figure 3.1. (From Vallance Jones, 1974).

Five parameters were used in this study to account for the system's emissions: four band brightnesses (the (1,0),(2,1),(3,2), and (4,3) bands) and one temperature which would be used for all four bands. As can be seen from Table 2.3, the fit of the (4,3) band was far from ideal (noted by the error). This could be due to a number of reasons: 1) low band brightness, 2) band origin near the limit of the measured spectrum, or 3) the abnormally high continuum at that end "stealling" some of the intensity from the (4,3) band. The band was left in the analysis because it was felt it would help

keep the continuum lower in magnitude. In any event, the poor fit of the (4,3) band requires leaving it out of the graphs that follow for clarity's sake.

Figure 4.4 shows a summary of the analyzed parameters. The scale for the three band brightnesses is on the left, while the scale for the temperature is on the right. Though it must be stressed that some of the variations in brightnesses and temperatures may be due to analytical fluctuations versus physical, general observations may be taken from the graphs. Quite possibly most of the variations may be later confirmed, through comparisons with other data, as real.

The most obvious feature of Figure 4.4 is that all three brightnesses follow nearly the exact same pattern. This is comforting and suggests a somewhat constant vibrational distribution with time. This is further investigated later in this section.

As seen with the atomic emissions, the pattern of brightnesses in Figure 4.4 shows about a 25 minute periodicity. It can also be seen that the temperature variation does not correspond to brightness variation. In fact temperature and brightness seem to be anticorrelated, noting their relationships at times 19.0 and 19.9 in the figure, in particular.

As mentioned shortly before, the band brightnesses varied similarly with respect to one another over time. This fairly constant variation allows us to make a vibrational population comparison. Cartwright et al. (1971)

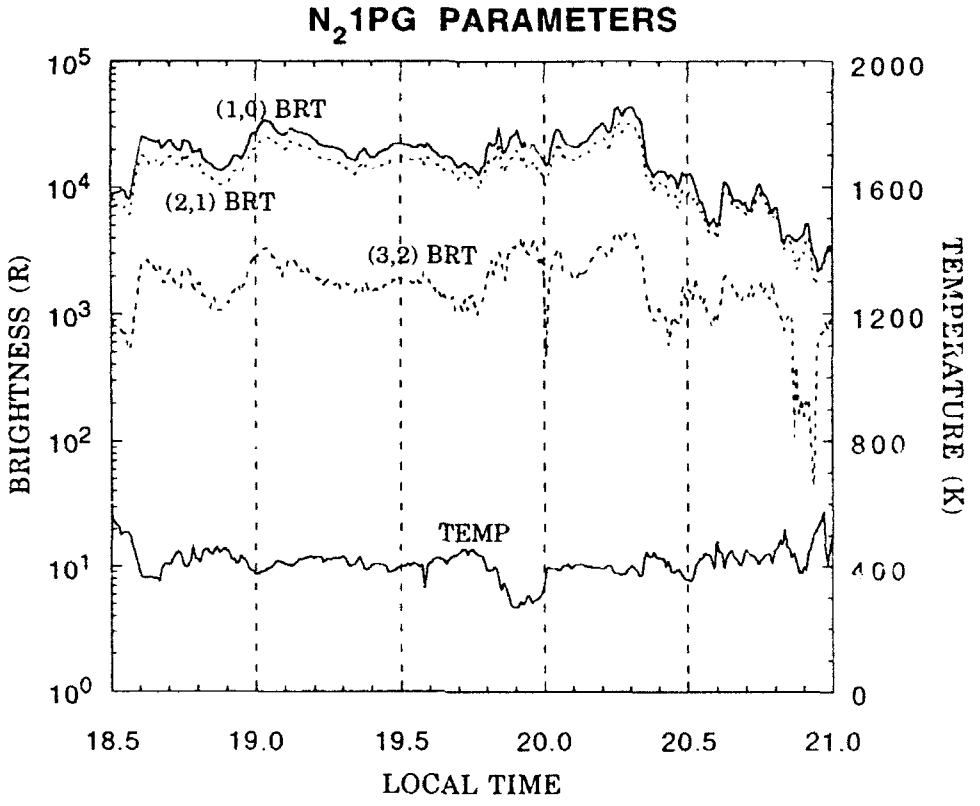

Figure 4.4 N_2 first positive band brightnesses and temperature recovered from the aurora measurements.

made a comparison of the vibrational population model they theorized with that of Shemansky. Here I have simply extracted the data from both models up to v=6, and superimposed the data derived from this study averaged over the period from 18.5 to about 21.0 EST for comparison purposes. Figure 4.5 shows the results.

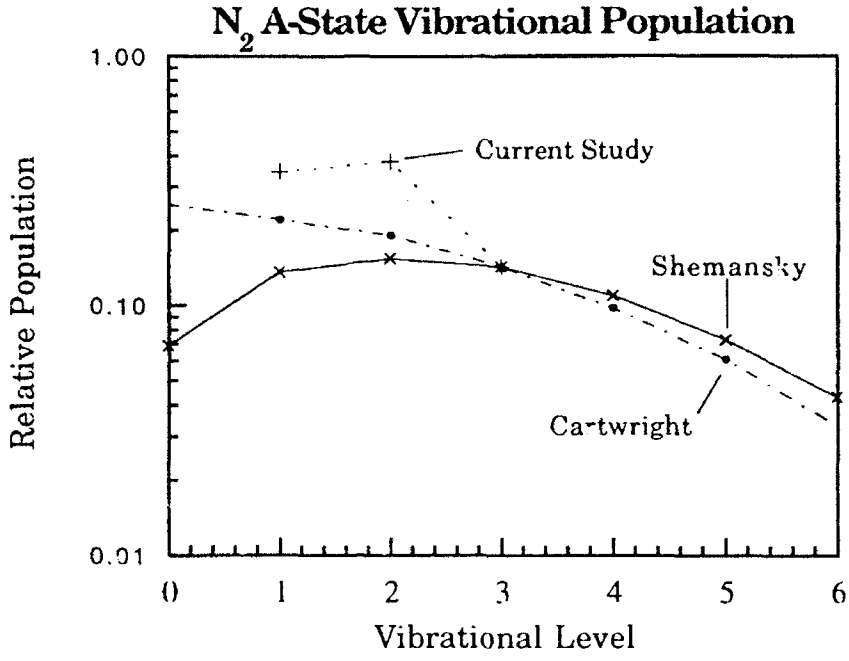

Figure 4.5 N_2 A-state vibrational population derived from first positive band brightness ratios. Populations are normalized to the v=3 level. Shemansky and Cartwright data taken from Cartwright et al., 1971.

As can be seen from the graph, the v=1,2 populations from this study seem to be too high when normalized to the v=3 level. This means that either the (1,0) and (2,1) bands are too bright, according to the two theories, or the (3,2) band is too dim. I believe the latter.

When viewing Figure 4.1, one can see that the high continuum mentioned earlier slopes from high to low wavelengths. Since the (2,1) and (1,0) bands lie to the high wavelength side of the (3,2) band, their band brightnesses are not affected as much as the (3,2) band by the sloped continuum. I believe that were it not for the unexpectedly high amplitude of the continuum, the ratios of the intensities of the (1,0) and (2,1) to (3,2)

bands would be much closer to the values predicted by Cartwright, in a qualitative sense, at least. However with the uncertainty of fit of the (3,2) band at 4%, and considering the slope of the data in Figure 4.5, agreement with Shemansky's vibrational distribution is not out of the question.

4.2.2 Infrared Afterglow

This system is one of the newest of the emissions known to occur in the aurora. Due primarily to overshadowing by first positive emissions, the infrared afterglow system, and consequently the upper state ($B'\ ^3\Sigma_u^-$), were not known about until the 1950's. The molecular constants required for band models to predict these emissions, were not available until around 1960. Since then, the N_2 IRA emissions have been analyzed numerous times (Gattinger and Vallance Jones, 1974, for example).

A view of the states involved in the transition ($B'^3\Sigma_u^- - B^3\Pi_g$) can be seen in Figure 4.3. Excitation of the N_2 molecule to the B'-state is primarily through energetic electron excitation. There are few radiative transitions to the B'-state, so cascading to this state should not occur often.

A large portion of this study was spent trying to decrease the magnitude of the continuum and to lower the value of χ^2. I believed the N_2 IRA system would resolve most of the continuum magnitude and high χ^2 problems. Much time was spent trying to develop a band model for the system. None could be located in time for use, when it was found that it would be possible to build such a model quite easily, noting that the $^3\Sigma$ - $^3\Pi$ transition is just the opposite of the first positive's: $^3\Pi$ - $^3\Sigma$.

Since E. Buscela (a PhD candidate at the University of Michigan) already had a model for the first positive system which was easily alterable, his model was chosen to be used for the origin of an N_2 IRA model. All that

was done to make the switch from first positive to IRA was to change the designation of the line strengths so that, for example, a rotational transition from level 2 to 1 of the $^3\Pi$ - $^3\Sigma$ became a 1 to 2 rotational level transition of the $^3\Sigma$ - $^3\Pi$. Therefore a P-branch of the first positive system became an R-branch of the IRA system, Q-branch line strength indeces stayed the same, and R-branches became P-branches. A test of the new model was accomplished and Figure 4.6 shows the comparison.

Figure 4.6 was created by convolving the individual rotational lines into the NIRS instrument function so that a channel ' channel comparison of model vs data could be made. Then a non-linear least squares fit of the band model to the data for both intensity and temperature was done. A band brightness of 1280 R and temperature of 208 K were found to give the model the best fit to the data. Molecular constants were obtained from Huber and Herzberg (1979).

It is evident that the model does a decent job of predicting the spectral shape and positions of the IRA bands, though I am not fully satisfied. The P, Q, and R-branch peaks appear to be displaced in wavelength somewhat (about 4 Å), and the intensity of the peaks are not in proper proportion with one another. In addition, the results of the analysis using the three IRA bands shown in Table 2.3 indicates the analytical error of the IRA bands is about twice that of other bands of similar brightnesses, and the consistency of the IRA recovered parameters were much less consistent than other species' parameters.

Nonetheless, the IRA model did improve the fit of the synthetic spectrum to the measurements somewhat, so the model was used as is, but with caution. The IRA band brightnesses and temperature recovered from the analysis were found to be too eratic to be shown in graphic format.

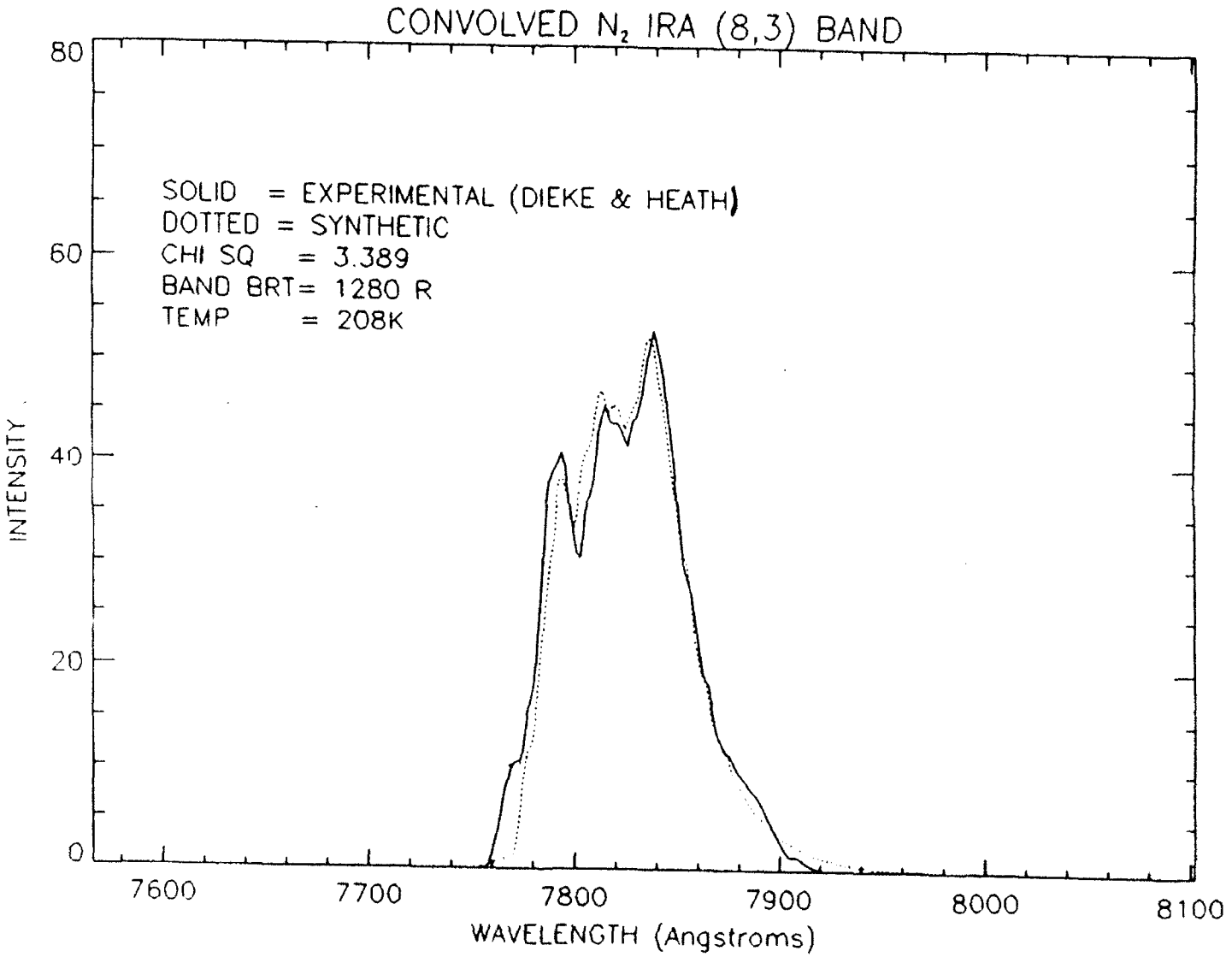

Figure 4.6 Comparison of modelled N_2 IRA with experimental data of Dieke and Heath (1960).

4.2.3 N_2^+ Meinel

This system was the only ion species analyzed in this study. It has been widely studied in the aurora and known to exist for quite some time. The primary source of production of the upper state of the Meinel band transition ($A\,^2\Pi_u - X\,^2\Sigma_g^+$) is electron impact ionization excitation (Rees, 1987):

$$e + N_2 \rightarrow N_2^+(A\,^2\Pi_u) + e. \qquad 4.1$$

For this system, only two parameters were chosen to be analyzed: the (5,3) and (4,2) band brightnesses. Since our spectral measurements do not have the sensitivity and resolution to produce a meaningful temperature, the temperature here was fixed at 600K.

Figure 4.7 shows the variation of the (4,2) and (5,3) band brightnesses with time. Although this graph has a linear scale on the vertical and the previous graphs have a log scale, one can still compare this graph with the others in a general sense and see the brightnesses follow the same basic pattern.

4.3 Oxygen

The only O_2 band system analyzed in this study is that of the atmospheric system. Although the $b^1\Sigma_g^+ - X^3\Sigma_g^-$ transition is a spin forbidden, magnetic dipole process, its appearance in the aurora is quite prominant. Observations of bands of this system were first taken from solar measurents back in the early 1800's (Krupenie, 1972). The energy levels involved in the transition are shown in Figure 4.8.

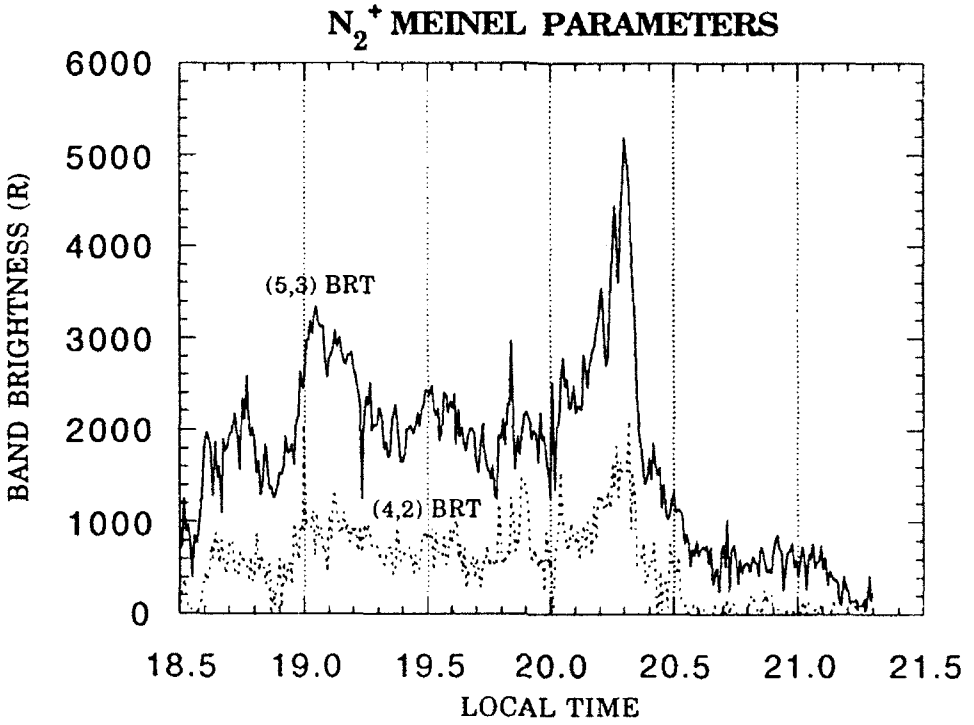

Figure 4.7 Time series of N_2^+ Meinel band brightnesses recovered from the aurora measurements.

The mechanism which produces the excited b-state of O_2 in the lower thermosphere is a chemical process. During nighttime and magnetically quiet periods, the emission occurs near 95 km and is produced from:

$$\begin{aligned} O + O + M &\rightarrow O_2^* + M \\ O_2^* + O_2 &\rightarrow O_2(b\,^1\Sigma_g^+) + O_2. \end{aligned} \qquad 4.2$$

At other times, such as in the dayglow and and the aurora, the production of $O_2(b^1\Sigma)$ is preceded by the production of $O(^1D)$:

$$
\begin{aligned}
O + e &\rightarrow O(^1D) + e \\
O_2^+ + e &\rightarrow O(^1D) + O \\
O_2 + h\nu &\rightarrow O(^1D) + O,
\end{aligned}
\qquad 4.3
$$

which leads to:

$$O(^1D) + O_2 \rightarrow O_2(b^1\Sigma) + O(^3P), \qquad 4.4$$

which then can radiate in the atmospheric system. Equation 4.4 is the main source of these emissions in the aurora.

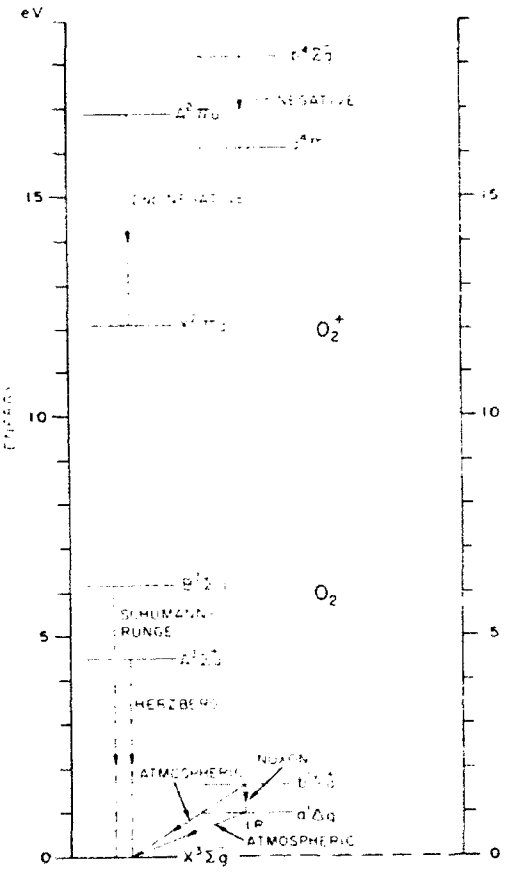

Figure 4.8 Potential energy levels and electronic band systems for O_2 and O_2^+ illustrated the same as Figure 3.1. (From Vallance Jones, 1974).

The lifetime of the $b^1\Sigma$ state is on the order of about 10 seconds. Since this state has such a long lifetime, many collisions with the ambient gas will take place before the emission occurs. We can then say the O_2 atmospheric temperatures recovered from the measurement will be pretty representative of the kinetic temperature of the ambient gas where the emission is taking place. This is not necessarily true for the recovered N_2 temperatures, which primarily represent the rotational distribution, owing to the short lifetimes of the upper states, but we can still say the N_2 temperatures approximate the kinetic temperature.

Figure 4.9 illustrates the time variation of the recovered O_2 atmospheric parameters. Three band brightnesses and two temperatures were chosen. Two temperatures were used in this case to see if more than one temperature could be recovered successifully, and indeed it could be done. This was not attempted with all other bands to keep computation time minimal.

The overall shape of the brightnesses and temperatures compare well among themselves and with those of the N_2 parameters as well. It is evident that the larger errors present in the weaker (2,1) and (3,2) bands creates slightly greater variability in both temperature and brightnesses.

It is interesting to note the relationship of the two temperature plots of Figure 4.9. The average temperature of the (0,1) band is 400K, while the average of the (1,2) and (2,3) bands' combined temperature is 625K. This is as we might expect. The higher vibrational states are more likely to exist at

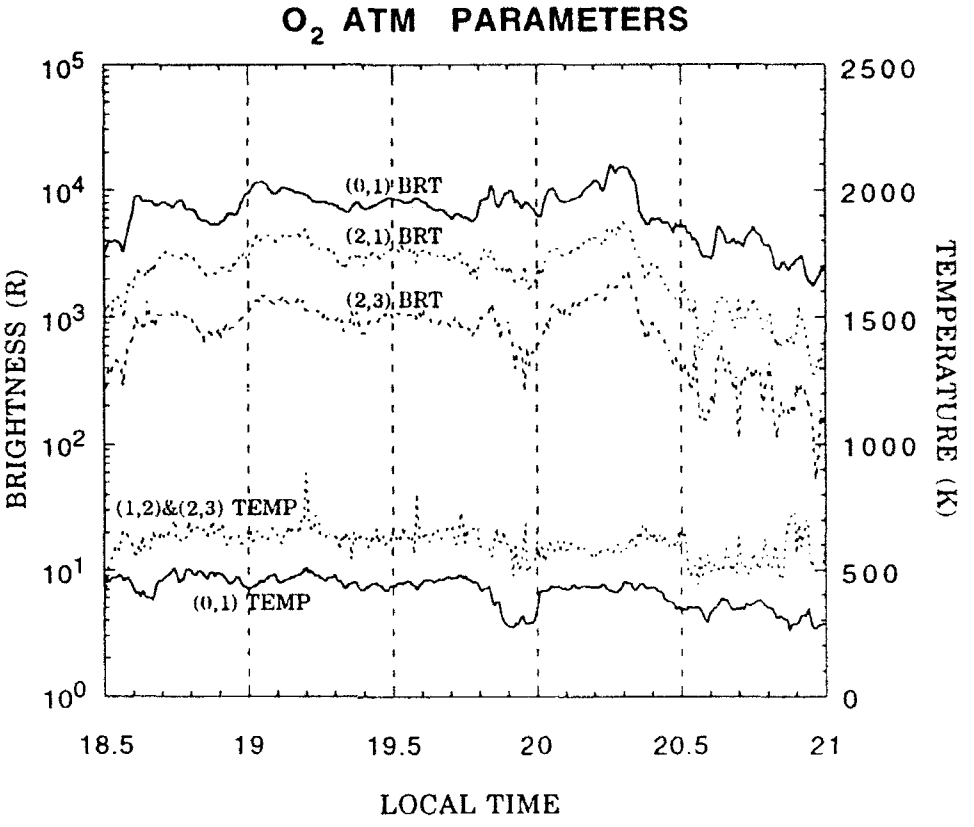

Figure 4.9 Time series of O_2 atmospheric band brightnesses and temperatures recovered from the aurora measurements.

higher altitudes in the thermosphere where there are fewer collisions that would deexcite, or quench, those states. We also know the ambient temperature increases with height in the thermosphere, where auroral emissions like the O2 atmospheric emissions originate. We would therefore expect the temperature of the (1,2) and (2,3) bands to be higher than the (0,1) band temperature.

4.4 Hydroxyl

The hydroxyl radical's (chemical abbreviation OH) emissions are a very widespread and dominant feature in any nightglow measurement of the infrared spectrum. Unlike the homonuclear molecules, OH has a permanent dipole moment that allows the molecule to make vibration-rotation as well as electronic-vibration-rotation transitions. Thus it can have more band emissions than diatomic molecules in the infrared spectrum.

The emissions, in the portion of the spectrum concerned with here, are due to overtone ($\Delta v>1$) transitions from vibrationally excited radicals in the ground electronic state of OH: $X\,^2\Pi_{\frac{3}{2},\frac{1}{2}}$. The primary source of the vibrationally excited radicals is the displacement reaction between H and O_3 (Bates and Nicolet, *1950*):

$$H + O_3 \rightarrow OH(v' \leq 9) + O_2 + 3.3eV \ . \qquad 4.4$$

The 3.3 eV of energy released by the reaction is enough to excite the radical up to and including the v'=9 vibrational level, sufficient to excite the molecule to the v'=6,7 levels investigated here.

Altitude profiles of the Meinel bands obtained by rocket borne instruments place the peak emission between about 85 and 90 km altitude. Since the rotational relaxation of OH is believed to be rapid enough to produce a thermal distribution of rotational populations, analysis of the rotational distribution yields the kinetic temperature of the ambient gas, as with the O_2 atmospheric system (Rees, 1989). Because the peak emission altitude of the OH Meinel bands is below the thermosphere, and the

emissions indicate ambient conditions of the 5 km altitude layer from where the photons originate, the OH Meinel bands are used extensively for investigating the effects of gravity wave propagation through the region.

Figure 4.10 shows the OH parameters recovered from the aurora measurements. It is immediately obvious that these emissons do not follow the same pattern of any of the species shown up to this point. This is as expected: since the peak emission altitude of the OH Meinel bands is near 85 km, and auroral electrons lose the bulk of their energy by inelastic scattering above 100 km, we would not expect OH Meinel emissions to immediately follow the others, which emanate from above the mesopause.

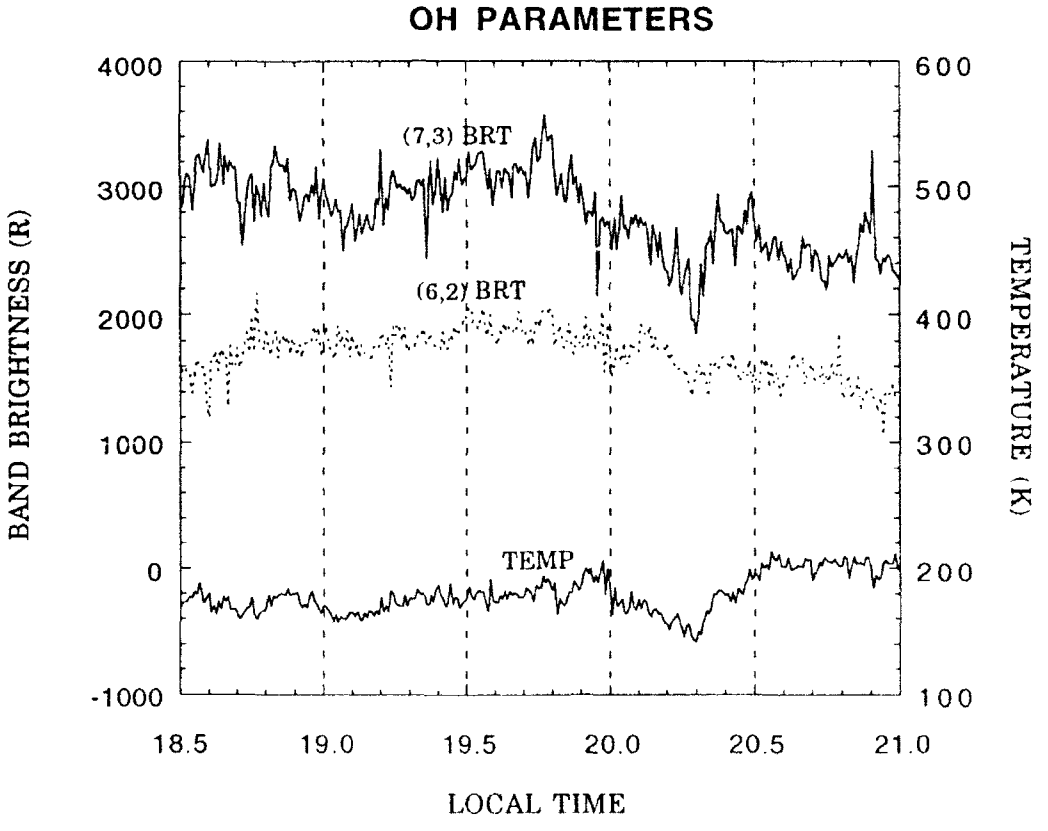

Figure 4.10 Time series of OH band temperature and brightnesses recovered from the aurora measurements.

4.6 Comparisons

4.6.1 Temperatures

One particularly useful indication temperature gives us is the altitude from which the emission is taking place. By using a model such as the empirical MSIS-86 model (Hedin, 1987), we can predict the temperature profile of the lower thermosphere. This will then allow us to make an estimation on the emission altitude by matching the temperature with a temperature profile from MSIS-86.

Figure 4.11 shows a plot of the temperature profile output from MSIS-86. The parameters input to the model to get this plot were: date=91313, time=0.0 UT (8 PM EST), F10.7=200, F10.7A=197, Ap=65, latitude=42, longitude=85 (Ann Arbor). Thus the profile is a snapshot, over Ann Arbor, MI, of the lower thermosphere at 8 PM on the evening of Nov. 8, the center in time of the aurora measurements.

Also included in Figure 4.11 are the four average temperatures during the aurora, recovered from the analysis, shown in previous plots. The N_2 IRA temperature again has been left out because of its high variability. The four temperatures have been assigned to an altitude on the MSIS-86 profile so that we can estimate where the peak of the emission layer is occurring.

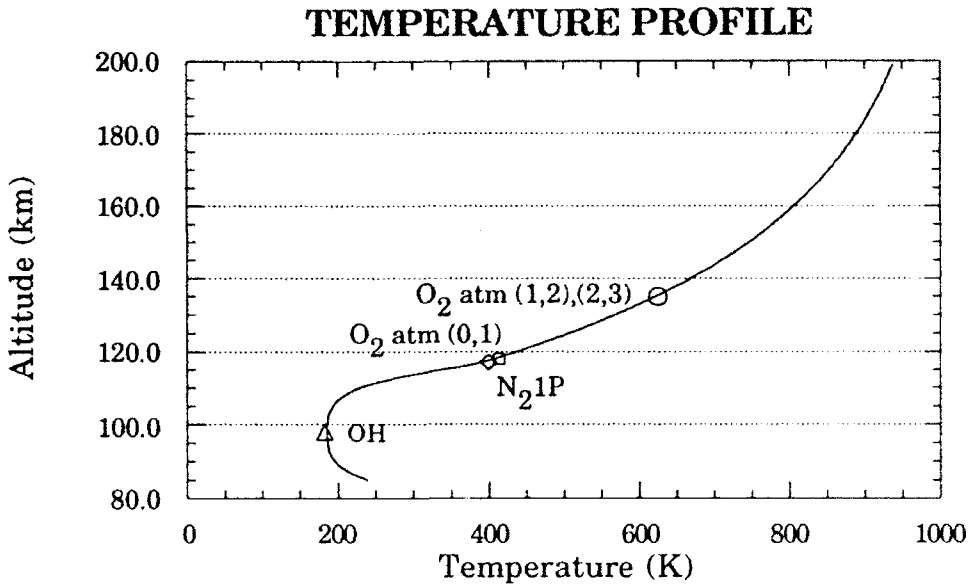

Figure 4.11 Temperature profile from 85 - 200 km. Profile is from the MSIS-86 empirical model, highlighted points on the graph are average species temperatures during the aurora.

Figure 4.12 is related to Figure 4.11, showing the variation of the recovered temperatures with time, with specific altitude (95,115,125,135,150) temperatures, as a function of time, added to show how the peak emission altitude of each species varied in that time period. The five altitudes levels were chosen simply on the basis of spacing.

If we assume that the changes in temperature of the species are primarily due to changes in the altitude of emission, we can see how the peak emission altitudes changed with time in Figure 4.12. The variation for the three thermospheric emissions is on the order of 20-30 kilometers, while the variation of OH's peak emission altitude is less than 10 kilometers between maximum and minimum peaks.

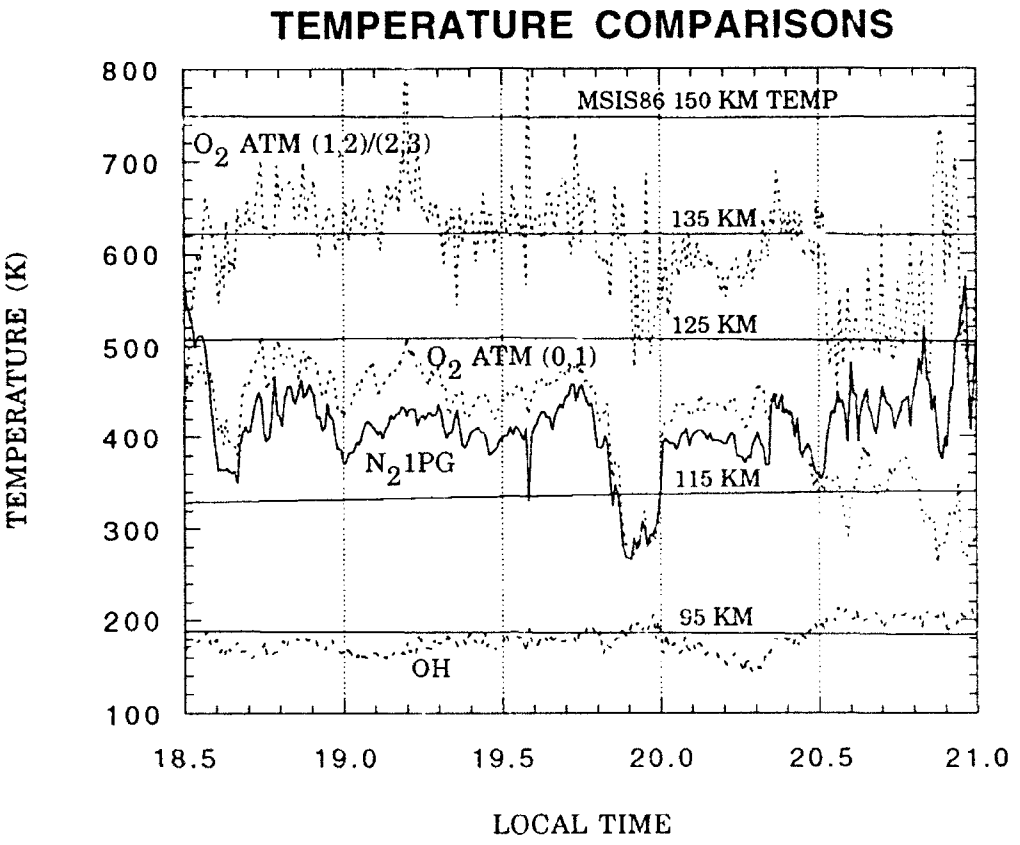

Figure 4.12 Comparison of species temperatures and MSIS-86 altitude temperatures.

Since the hydroxyl radical's emission is largely unaffected by the auroral electrons, it's temperature variation is probably primarily due to actual changes in kinetic temperature and secondarily to emission altitude. The OH temperature variation is considered to be dominated by upward propagating gravity waves, and a spectral analysis on the temperature variation would yield useful information on the influence of the waves.

One last note on the hydroxyl emission: as was noted earlier, the peak emission altitude of OH is generally considered to be between 85 and 90

km, as measured by rocket-borne instruments. The temperature recovered from the aurora measurements averaged to about 180K, but the MSIS-86 model predicted a temperature at 90 km to be 196 K, and a minimum temperature at the mesopause (95 km) to be 186 K. Thus the recovered temperatures from the OH bands is lower than any altitude's temperature predicted by MSIS. It is known that the model's accuracy is + or - 10-15% (about 3 K). The recovered temperature error is probably good to within about 5 K. With these error limits in mind, the recovered temperatures still suggest a peak emission altitude greater than 90 km.

4.6.2 Temperature vs. Brightness

Interesting observations can be made when comparing species brightness with it's temperature, as done before, but with a little more detail. Figures 4.13 and 4.14 show band brightnesses versus species temperature for O_2 and N_2 respectively.

We noted before that the temperatures and brightnesses seemed to be anticorrelated, or out of phase by about 180 degrees. From the figure above, with the scales expanded, one can see this is definitely the case. The two plots are not perfectly out of phase, but close to it over most of the period, within about three minutes.

Our results suggest that when emissions are their brightest, which is when the auroral electron flux is greatest, the ambient temperature is lowest. This notion can be explained in the following way. A burst of highly energetic auroral electrons precipitating downward can penetrate deeper into the atmosphere than a burst of less energetic electrons. This is because more highly energetic electrons can experience more inelastic

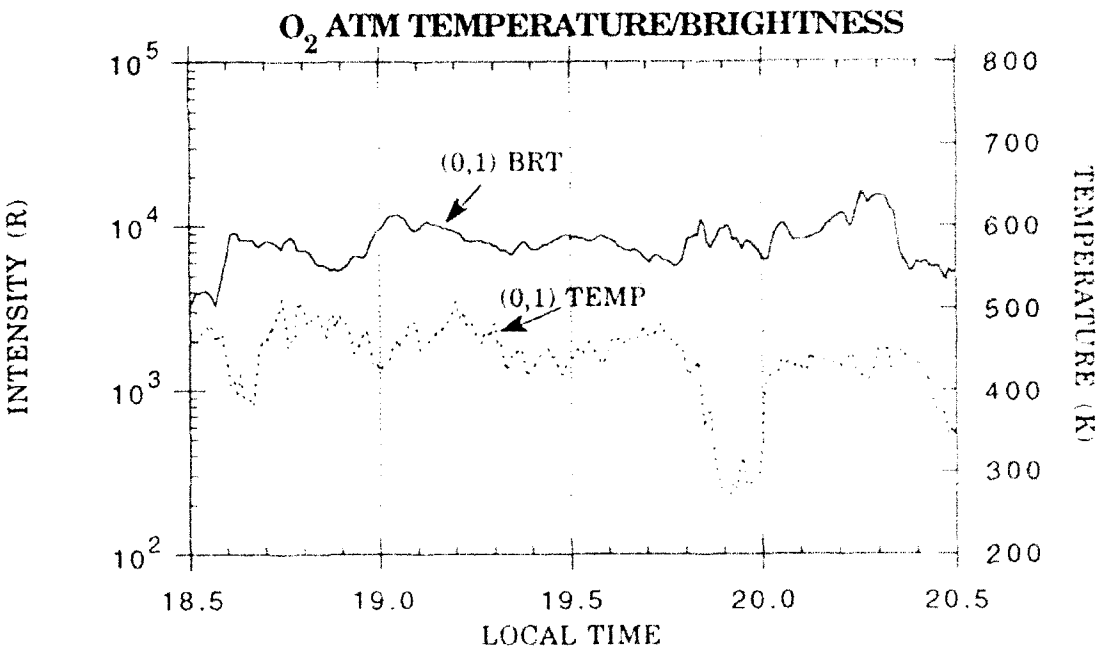

Figure 4.13 O_2 Atmospheric (0,1) band brightness versus temperature.

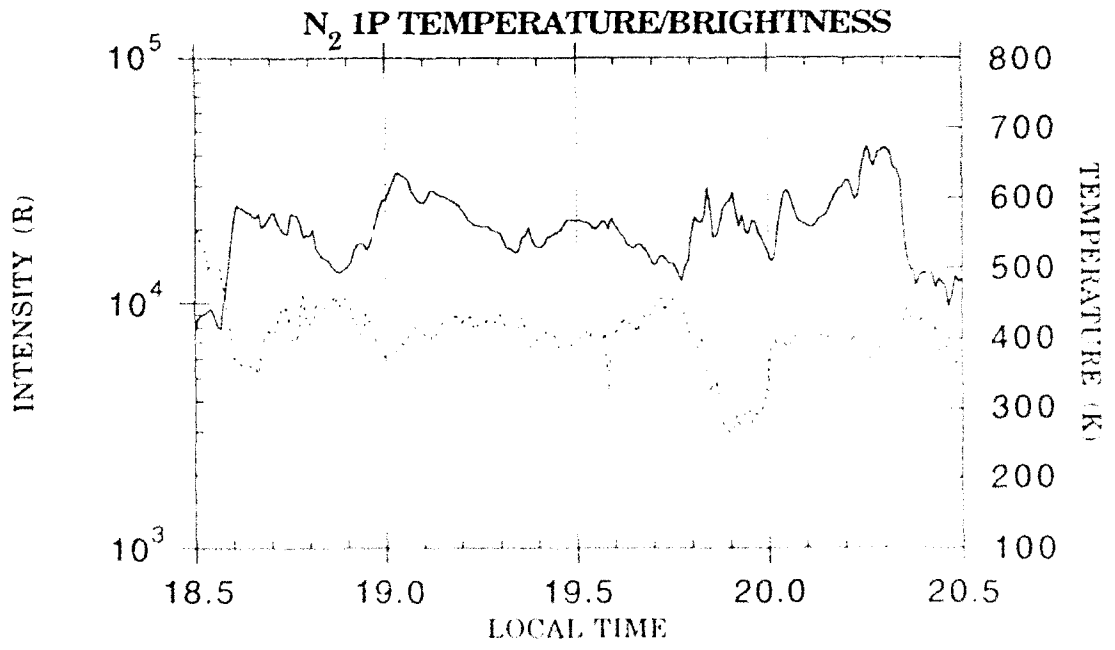

Figure 4.14 N_2 first positive (1,0) band brightness versus temperature.

collisions with ambient particles on their way downward through the earth's atmosphere, before giving up all their excess kinetic energy, than less energetic particles can. So the greater the average energy of an auroral electron distribution, the deeper the energy can penetrate, and the peak emission will come from a lower altitude due to the greater density at lower altitudes. In addition, the brightness of the aurora is determined by the magnitude of the flux of auroral electrons (expressed in terms of ergs/cm^2/sec in cgs units). Since the recovered data suggests lower temperatures (and therefore emission altitude) accompany higher intensities in the aurora, then the fluxes of more energetic electrons must have come in greater numbers also.

To summarize, 1) the temperature suggests a penetration depth of electrons. 2) The penetration depth suggests the characteristic energy of the auroral particles. 3) The magnitude of the flux of auroral electrons affects the brightness of the aurora. One can therefore use the recovered temperatures and brightnesses to estimate the characteristic energy and flux of auroral particles through the use of a model.

This concludes chapter 4 and the entire study's analysis of the aurora measurements. The final chapter, chapter 5, will restate what I have already presented, and will suggest areas where improvement can be made so that an even more complete analysis of the data, and verification of results can be achieved.

CHAPTER 5

CONCLUSIONS

5.1 General Remarks

On the evening of November 8, 1991, a moderate intensity auroral event was observed over Ann Arbor, MI (42 N, 85 W), as well as many more equatorward locations. Since this region is outside the auroral zone, the event is a fairly uncommon one at this location, and if the measurements had been taken inside the auroral zone, the intensities would have been extremely bright, much more so than measured in Ann Arbor. This fairly unusual event for this region was measured by the University of Michigan's Near-Infrared Spectrometer from 6:30 to 12:00 pm EST continuously for integration periods of 30 seconds. A description of the instrument and it's CCD detector was given in chapter 1.

The instrument resolution is about 13 Å, and NIRS was set up to measure the spectral region of approximately 8400-8900 Å for a nightglow study when the unexpected auroral event occurred. With a 30 second integration time, and considering only photon statistics, the measurement

readings at each of the 384 data channels are accurate to within +/- 0.5% for brighter periods and +/- 1.5% for less intense periods.

Retrieval of useful emission parameters such as atomic line intensities, molecular band brightness, and molecular band temperature require analysis of the data and the creation of a synthetic spectrum, which accounts for all emissions believed to exist in the measurement. The inclusion of molecular emissions in the synthetic spectrum requires a band model for each type of transition. The band model output hundreds of individual rotational lines emitted due to the molecule's transition, based on the inputted total band brightness and temperature.

Once the entire synthetic spectrum is constructed from atomic and molecular parameters, then convolved, analysis of the data through the use of a least squares technique is required, so that the best possible fit of the synthetic spectrum to the measurement is found. A non-linear least squares technique discussed in chapter two was used for this study to recover a total of 31 parameters from the measurements, including low-end and high-end continuum brightness parameters used to "fill in the gaps".

The iterative non-linear least squares technique was used on the entire evening's measurements, about 600 30-second frames. The vast majority of this study concentrated on the time period from 6:30 to 9:30 pm EST, when the aurora was at it's brightest. Once I was satisfied with the goodness of fit of the synthetic spectrum to the measurements, judged primarily from the value of chi-squared, investigation of the recovered parameters for physical insight was begun.

The primary purposes of this study, then, was to build a non-linear least squares fitting technique that was flexible enough to change allow changes in parameters with minimal effort, arrive at a suitable synthetic

spectrum, and attempt to verify physically what the recovered parameters implied.

5.2 Results

Chapter 3 discussed features found in the atomic species' emissions. One oxygen and nine nitrogen lines, for a total of ten, atomic emission lines were recovered from the measurements. The most dominant lines in the 8400-8900Å spectral range measured, in order of most to least intense, were: OI 4 8446Å, NI 1 8683, NI 1 8680. These and the seven other atomic lines were plotted as a function of time. All the lines showed a similar intensity versus time pattern, with a periodicity of about 25 minutes, which was apparently driven by the variation of the flux of auroral electrons.

An attempt was made to verify the relative strengths of some of the nitrogen lines measured. To do so, the ratio of lines with the same multiplicity within the same electronic transition, were compared with the ratio of the Einstein transition probabilities (from Wiese, et al., 1966). The results showed the 8594/8656Å intensity ratio to be lower than the expected value by a factor of about 1/2, and the 8683/8719Å intensity ratio to be too high by a factor of 3.5.

Chapter 4 discussed the molecular species' parameters recovered from the aurora data. A total of 14 molecular band brightnesses and 5 band temperatures were recovered from the data. The molecular species analyzed in this study, in order of total intensity of emission, are: N_2 1st Positive (N_2 1PG), O_2 Atmospheric (O_2 Atm), N_2 Infrared Afterglow (N_2 IRA), N_2^+ Meinel (N_2^+ M), and the hydroxyl radical (OH).

The N_2 1PG system was the most useful system of all to this study, because of the number of vibration-rotation bands (the (1,0), (2,1), (3,2), and (4,3) bands) in the measured spectrum. The (4,3) band was evidently too weak, or too far off of the low wavelength side of the spectrum to be recovered with any reliability. The other three bands, however, were consistent enough to allow a study of vibrational population to be accomplished, using data taken from Cartwright, et al. (1971).

Our results gave higher populations for the v=1,2 levels, when normalized to v=3, than either Cartwright's or Shemansky's modeled vibrational population in the aurora, by about 10% and 20%, respectively. While the values of the populations agreed with Cartwright's model better than Shemansky's, the slope of this study's vibrational population, however, tended to agree with the model of Shewmansky better. It was suggested that some of the disagreement of the results with both models may have been due to the unexpectedly high value of the recovered continuum at the low wavelength side of the spectrum.

The N_2 IRA system was added to the list of parameters when it was noted how many bands this system had in the spectrum. A total of six bands exist in or near the 8400-8900Å range. It was thought that some, if not all, of these bands would lower the high continuum values and also enhance the goodness of fit by lowering χ^2. After trying to fit all the bands, with many different combinations, it was found that the system only slightly helped lower the continuum values and χ^2. In addition, the error of fitting and consistency of the recovered IRA parameters prohibited meaningful examination of the parameters. It was felt that improvement of the band model developed may improve conditions.

The N_2^+ Meinel system has two bands which emit in the spectrum studied. These two bands were analyzed with a fixed temperature of 600K. A time series of the band intensities was presented. It showed a similar band brightness versus time pattern as the other species.

The O_2 atmospheric system's three bands were fitted using two temperatures: one corresponding to the (0,1) band only, and one corresponding to the (1,2) and (2,3) bands. The results give a higher temperature for the (1,2)/(2,3) bands than the (0,1) band. This suggests a higher peak emission altitude for the higher vibrational states (v'=1,2) than the v'=0 vibrational state.

Two bands of the hydroxyl radical's (OH) Meinel system were analyzed from the measurements. The peak emission altitude of OH (85-90 km) precludes these emissions from being enhanced by auroral electrons. The recovered band brightnesses and temperatures did not vary in a way which was similar to that of species associated with the aurora.

Comparisons of different species' temperatures were made with reference to the MSIS-86 temperature profile. The average altitude of peak emission for each species was: OH-95 km, N_2 1PG- 115 km, O_2 atm (0,1)- 117 km, and O_2 atm (1,2)/(2,3)- 135 km. The OH emission altitude, in particular, is notably higher than anticipated.

A comparison of species temperatures with MSIS-86 altitude temperatures was made, in order to show variation of peak emission altitude, assuming there is little change in kinetic temperature taking place. Results suggest variations of emission altitude are about 25 km for most species, while the variaton of hydroxyl is less than 10 kilometers between maximum and minimum values.

When closely comparing species brightness and temperature versus time, one can see the recovered data shows that temperature is out of phase with band brightness. Since, from the discussion in section 4.6.2, we know that species temperature can yield the characteristic energy of auroral particles, and the magnitude of the flux of auroral electrons determines brightness. The out of phase relationship between temperature and brightness suggests a higher characteristic energy of auroral electrons accompanied greater periods of flux of electrons during these measurements.

5.2 Areas for Improvement

As suggested in various places throughout this writing, there are a number of places where improvement can be made to more fully perfect recovery of emission species parameters, and to carry further the use of recovered information to further ends. The most immediate of which is the modelling of the auroral particle flux using temperatures and brightnesses recovered from the data. This, when combined with other measurements, can lead to a greater understanding of cause and effect of the many variables associated with the aurora.

Improvements on the fitting of parameters can be made. As noted earlier, much time was devoted to attempting to lower χ^2 and continuum magnitudes. I believe that most of the problems with the fitting is on the low wavelength side, due to the magnitude of continuum being so high on that end, and because of the poor fit of the synthetic spectrum to the measurement near 8430Å, as depicted in Figure 4.1. There are two possible explanations for the less than ideal fit: 1) there is one or more atomic and/or

molecular species which are important here that have not been included in the analysis, 2) there may be some internal scattering of radiation in the NIRS spectrometer which may be creating "white noise" in the measurements.

The first option, that there may be species left out of the analysis, is a tough one to solve. Possible species which have not been tried, due to the belief that they would have a very minor effect, are: the OI 4 8426 Å atomic line, and the (0,5) band of the O_2^+ 1NG (first negative ground) system. The other 11- NI 1 and NII atomic lines may improve fitting at other parts of the spectrum.

The possibility of white noise, or internal scattering of light in the spectrometer, can be partly justified when examining Figure 5.1. It shows how χ^2, a measure of goodness of fit, varies with time. An ideal fit would have a χ^2 value of 1. The OI 8446 line is added as a reference, to show the intensity of the aurora with time. One can see that when the aurora brightens, as indicated by the 8446 line, the value of χ^2 goes up as well, and during the dimmer periods the value of χ^2 goes down.

It is obvious that during brighter periods there will be more scattering of white light in the spectrometer, and during less bright periods there will be less scattering, if it is indeed occurring. Since the instrument has only been used, up to November 8, 1991, to measure much less intense nightglow, this was never noticed to be a problem, and nothing yet is conclusive to prove scattering is a problem. Even if scattering is the culprit, there is nothing practical that can be done to the data to correct for it.

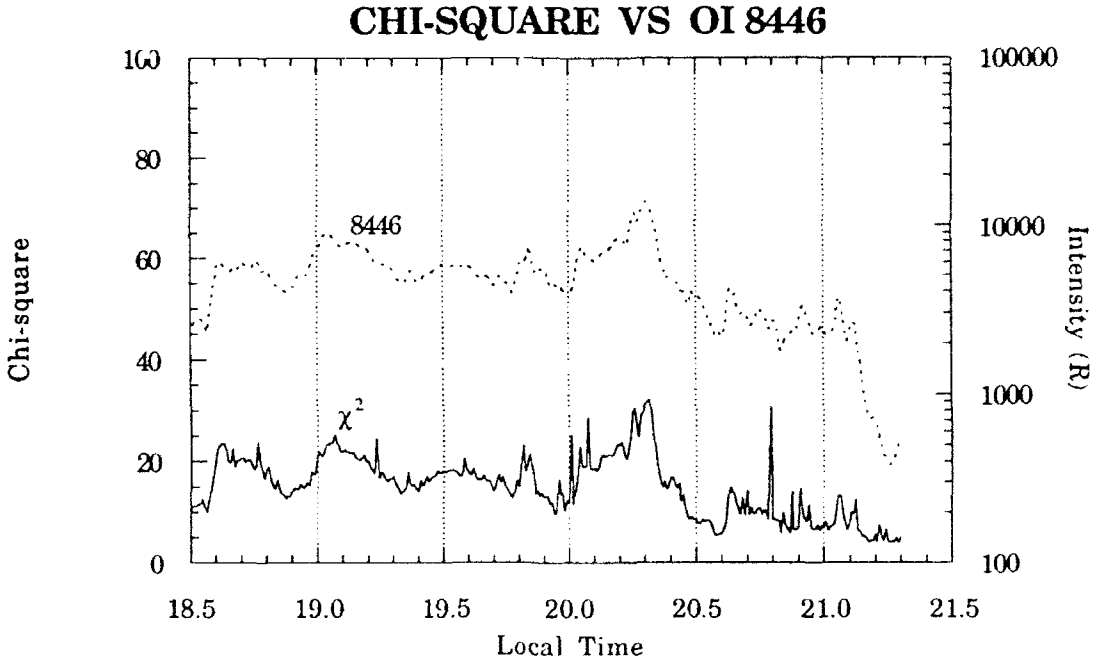

Figure 5.1 Plot of c^2 and OI 8446 versus local time (EST).

The N_2 IRA model is another possible source of improvement. As seen in Figure 4.5, the modelled spectrum does not fit the experimental spectrum perfectly. Again there was insufficient time to fully investigate the model's output, so it was necessary to use it as is.

APPENDIX

SOURCE CODE

The source code for the analysis is listed here for reference. The code is definitely research-grade and was not written specifically for optimum performance. Instead it was written so that molecular and atomic emission parameters could be added and changed without a great deal of code manipulation. Before listing the code, a few helpful hints will be passed along so that someone else may benefit.

Convergence. The first problem I ran into was that I could not get the chi-square fitting routine, SPEC_FIT, to converge: the value of chi-squared just got worse and the recovered parameters were useless. The problem was that when trying to analyze for both band brightness and temperature of a particular molecular species using band models, you need to be in the vicinity of the minimum of parameter space. Both temperature and brightness cannot be arbitrarily set. I got around this problem by "hard-wiring" in reasonable temperatures so that accurate brightnesses could be attained. Upon saving these parameters to a file, I then adjusted the program to read in the file of parameters, and also allowed for temperatures to then be analyzed along with the other parameters. Convergence was then not a problem.

Data Spikes. Another problem was that the raw NIRS data had "spikes" in it. These spikes were apparently from very energetic photons which were able to by-pass the baffles and made their way to the CCD. Though only about 10% of the frames had spikes in them, it did affect some of the fitting quite a bit, and the spikes seemed to be more common during the brighter periods. The spikes affected not only the channel where the photon was absorbed, but also about 2 channels to either side of the primary channel, and many times there were multiple spikes in a single frame of data.

To minimize the affects of the spikes on the fitting, any number of routines can be applied. I chose to use a simple averaging scheme. Once the data file was read and returned to the main program, I inserted a series of loops to check each frame and channel for spikes: anything greater than 100 counts over the channel's reading at 3 frames to either side of the channel being checked, then the 5 data points within that range would be replaced by a time average of each channel. This time average was obtained by adding the preceding and succeeding frame's reading for that particular channel, and dividing by 2. This smoothing process seemed to work quite well. For the worst fitting frame before the process was added had a chi-squared value of about 75. After the routine was added, chi-squared was brought down to under 30, which was close to values obtained from nearby frames which had no spikes in them.

Negative Parameters. A third problem, though a very minor one, was that the least squares fitting routine had no concept of reason- often parameters (temperatures and brightnesses) would optimize to negative values. I suppose negative brightness may imply absorption, but negative temperatures are difficult to grasp. Though this generally occurred for

only the weaker emissions and did not affect the fit greatly, it did allow the program to "cheat". This was gotten around by resetting negative parameters to an arbitrary, low number. The value of 1.0 was used in this study. This prevented the program from "cheating" by using better fitting negative parameters and did not cause any known problems on succeeding iterations when done properly.

Source Code Listing

```
CCCCCCCCCCCCCCCCCCCCCCCCCCCCCCCCCCCCCCCCCCCCCCCCCCCCCCCCCCCCCCCCCCCCCCC
C
C       PROGRAM:   SPEC_ANAL.FOR
C
C       PURPOSE:  Main driver for the SPEC_FIT subroutine.  First calls GET_DATA subroutine to
C                 retrieve the NIRS measurement data. It then sends the data for spectral fitting to
C                 SPEC_FIT.  The fitting subroutine uses a non-linear least squares iterative technique to
C                 find the best fit of the fitting parameters specified by the user to the data.  Recovered
C                 parameters are atomic emission line intensities, molecular band temperature, and band
C                 brightness.  Spectral range:  8400-8900 A.
C
C       EXTERNAL SUBROUTINES CALLED: MATINV, ATMOS_CROSS, OH_SPEC,
C                 OH_SPEC1, N21P
C
C       MAIN VARIABLES USED IN PROGRAM:
C                 NCH:  number of channels of the NIRS instrument
C                 NPRM:  number of parameters to be recovered from the data
C                 N:  number of atomic lines analyzed
C                 DT:  integration period
C                 MXFRM: maximum number of frames to be read (for dimensioning only)
C                 WAVE:  reference wavelength.  Determines where the spectrum begins (channel 1) at the
C                        high end since wavelength decreases as the channel number increases
C                 CNT:   array containing the number of counts (corrected) arranged by channel, frame no.
C                 EMI:  synthetic spectrum counts which best fits the data based on specified parameters:
C                        output from SPEC_FIT to compare with data (COUNT).
C                 COUNT:  an array of the current frames' data from CNT to be sent to SPEC_FIT.
C                 A:  array of recovered parameters.  Dimensioned to NPRM.
C                 SIGMA: array of errors of the A parameters.  Dimensioned to NPRM.
C                 LINES:  array of atomic lines to be analyzed.
C
C       Designed by:      Thomas J. Smith                15 January 1992
C       Written by:       Thomas J. Smith
C
CCCCCCCCCCCCCCCCCCCCCCCCCCCCCCCCCCCCCCCCCCCCCCCCCCCCCCCCCCCCCCCCCCCCCCC


      PARAMETER (NCH=384, NPRM=31, N=11, DT=30.0, MXFRM=750)
      REAL*8  WAVE
      REAL    CNT(NCH+1,MXFRM),EMI(NCH),TIME(MXFRM),CCD(MXFRM)
      REAL    COUNT(NCH),DK(MXFRM),A(NPRM),SIGMA(NPRM),LINES
      INTEGER SPFLG(MXFRM)

     COMMON /OH/ID_OH,DARK,LINES(N)
     COMMON /TRANS/WAVE
     DATA WAVE/ 8906.249D0/
     DATA LINES/ 8446.50, 8567.74, 8594.00, 8629.24, 8655.89,
     >           8680.28, 8683.40, 8703.25, 8711.70, 8718.83, 8828.89/


C       Allow for different OH molecular data to be used.

C     WRITE(6,1020)
C 1020 FORMAT(1X,'ENTER THE SOURCE OF OH TRANSITION PROBABILITY:'/,
C     &       1X,'0: MIES;  1:TURNBULL AND LOWE;  2: LANGHOFF: ',$)
```

```
C     ACCEPT *, ID_OH
      ID_OH = 0


C       Get the data to analyze

      CALL GET_DATA(DT, CNT,NUMFRAM,TIME,DK,CCD)

      PRINT *,'        FRAME    TIME     CHI SQ   CCD TEMP   # LOOPS '

C       Now check data for spikes by finding an avg count from 3 channels either side, and avg of 1
C       channel  either side of each point.  If the data is greater than 100 counts (RLIM) more than the 2
C       averages then the data point is assigned the value of the time average (AVFRAM).

      RLIM=100.
      DO I=2,NUMFRAM-1
        DO J=3,NCH-3
          AVCHAN = (CNT(J+3,I)+CNT(J-3,I))/2.
          AVFRAM = (CNT(J,I+1)+CNT(J,I-1))/2.
          IF ((CNT(J,I).GT.AVCHAN+RLIM).AND.
     &         (CNT(J,I).GT.AVFRAM+RLIM)) THEN
            IF ((CNT(J,I).GT.CNT(J+1,I)+RLIM).AND.
     &           (CNT(J,I).GT.CNT(J-1,I)+RLIM)) THEN
              CNT(J-2,I) = (CNT(J-2,I+1)+CNT(J-2,I-1))/2.
              CNT(J-1,I) = (CNT(J-1,I+1)+CNT(J-1,I-1))/2.
              CNT(J,I) = AVFRAM
              CNT(J+1,I) = (CNT(J+1,I+1)+CNT(J+1,I-1))/2.
              CNT(J+2,I) = (CNT(J+2,I+1)+CNT(J+2,I-1))/2.
              SPFLG(I) = 1
            ENDIF
          ENDIF
        ENDDO
      ENDDO

C       Loop over the number of frames of data (NUMFRAM) for analysis.  Reassign the array of
C         intensities CNT to the vector COUNT then pass it to SPEC_FIT.

 5    DO 100 I=1,NUMFRAM
        DO 10 J=1,NCH
 10       COUNT(J) = CNT(J,I)
          DARK = DK(I)

          CALL SPEC_FIT(COUNT,DT, A,SIGMA,EMI,NLOOPS,XSI,IERR)

          IF (I.EQ.1) THEN
            OPEN(UNIT=2,FILE='[TSMITH.AURORA.DATA]31PRMSPEC.DAT',
     &           STATUS='NEW')
            OPEN(UNIT=3,FILE='[TSMITH.AURORA.DATA]31PRM.DAT',
     &           STATUS='NEW')
          ENDIF

          IF (IERR.EQ.0) THEN
                WRITE(6,'(10X,I5,3F10.3,2I8)')I,TIME(I),XSI,CCD(I),NLOOPS,SPFLG(I)
            WRITE(3,'(F8.3,F7.2,F6.1,2I3,10F8.1)')TIME(I),XSI,CCD(I),
     &                    SPFLG(I),NLOOPS,(A(J),J=1,10)
                WRITE(3,'(27X,11F8.1)')(A(J),J=11,NPRM)
          ENDIF
 100    CONTINUE
```

```
      CLOSE (2)
      CLOSE (3)
      STOP
      END

CCCCCCCCCCCCCCCCCCC  SUBROUTINE GET_DATA  CCCCCCCCCCCCCCCCCCCCCC

    SUBROUTINE GET_DATA(DT, CNT,NUMFRAM,TIME,DARK,CCD)

C       PURPOSE:  Reads in the NIRS spectrometer data file by time (frame) then corrects the data for
C                 dark counts and instrument bias (read error).
C
C       MAIN VARIABLES:
C       DARK:  array of dark counts measured by the (covered) 385th channel during each frame
C       CCD:  array of CCD temperatures calculated from the dark counts
C       CNT:  array of counts measured, corrected for dark counts and bias.  Arranged by channel, frame
C
CCCCCCCCCCCCCCCCCCCCCCCCCCCCCCCCCCCCCCCCCCCCCCCCCCCCCCCCCCCCCCCCCCCC

      PARAMETER (NCH=384, MXFRM=750)
      REAL    CNT(NCH+1,MXFRM),C0(NCH+1),C1(NCH+1),H(NCH+1)
      REAL    TIME(MXFRM),DARK(MXFRM),COUNT(NCH+1,MXFRM),CCD(MXFRM)
      INTEGER*4 STATUS,LIB$GET_LUN
      INTEGER DARK_UNIT,BIAS_UNIT,HOUR,MIN

C       First open instrument calibration and measurement data files.

    STATUS = LIB$GET_LUN(DARK_UNIT)
    OPEN (UNIT = DARK_UNIT,
    &       NAME='[TSMITH.AURORA.DATA]MATIS_DARK_COEF_384.DAT',
    &       READONLY, TYPE='OLD')
    STATUS = LIB$GET_LUN(BIAS_UNIT)

    OPEN (UNIT = BIAS_UNIT,
    &       NAME='[TSMITH.AURORA.DATA]BIAS_384.DAT',
    &       READONLY, TYPE='OLD')

    OPEN (UNIT = 1,
    &       NAME='[TSMITH.AURORA.DATA]SPECT.DAT',
    &       NAME='SPRL1::HRD$SCR:[YEE]NOV0891.DAT',
    &       READONLY, TYPE='OLD')

     PRINT *,' '
     PRINT *,'       READING INSTRUMENT DATA...'

C       Read the dark counts and bias.

    DO K = 1,NCH+1
     READ(DARK_UNIT,*) C1P,HP,C1(K),H(K)
     READ(BIAS_UNIT,*) KK,C0(K),C0_ERR
    ENDDO

    NUMFRAM = 0
    TIME_OLD = 999.0
    INDEX = 0

    PRINT *,'       READING DATA FILE...'
```

```
C       Loop to read in measurement data, check for bad frame (COUNT=16383)

      DO 900 I = 1,MXFRM
       NUMFRAM = NUMFRAM + 1
       READ(1,*,END=950) IA,IB,IC,ITIME,ICH,CCT,N,TP,
     &          (COUNT(J,NUMFRAM),J=1,NCH+1)
       IF (ITIME.LT.1200) ITIME = ITIME + 2400
       IF (ITIME.LT.1800) THEN
        NUMFRAM = NUMFRAM - 1
        GO TO 900
       ENDIF

       DO J = 1,NCH+1
        IF (COUNT(J,NUMFRAM).EQ.16383) THEN
         NUMFRAM = NUMFRAM - 1
         GO TO 900
        ENDIF
       ENDDO

       HOUR = ITIME/100
       MIN = ITIME - HOUR*100
       MIN = HOUR*60 + MIN
       TIME(NUMFRAM) = MIN/60.0
       IF (TIME(NUMFRAM).EQ.TIME_OLD) THEN
        TIME(NUMFRAM) = TIME(NUMFRAM) + INDEX*0.008333
        INDEX = INDEX + 1
       ELSE
        INDEX = 1
        TIME_OLD = TIME(NUMFRAM)
       ENDIF
  900  CONTINUE
  950  NUMFRAM = NUMFRAM - 1
       CLOSE (1)
       CLOSE (DARK_UNIT)
       CLOSE (BIAS_UNIT)

       PRINT *, '          TOTAL FRAMES READ =',NUMFRAM

C       Subtract out the instrument bias, then calculate CCD temp and DARK count, then subtract out the
C       dark count.

      DO I = 1,NUMFRAM
       DO J = 1,NCH+1
        CNT(J,I) = COUNT(J,I)- C0(385)
       ENDDO

       CCD(I) = - 50.0 - H(385)*LOG(CNT(385,I)/(C1(385)*DT))
       DARK(I) = DT*C1(1)*EXP(-(CCD(I)+50.0)/H(1))

       DO J = 1,NCH
        CNT(J,I) = CNT(J,I)-DT*C1(J)*EXP(-(CCD(I)+50.0)/H(J))
       ENDDO
      ENDDO
      RETURN
      END
```

```
CCCCCCCCCCCCCCCCCCCCCC    SUBROUTINE SPEC_FIT  CCCCCCCCCCCCCCCCCCCCCC

      SUBROUTINE SPEC_FIT(Y,DT, A,SIGMA,F,NLOOPS,XSI,IERR)

C       PURPOSE:
C       Non-linear least squares fitting of data to derive parameters such brightness and band temperature.
C       Uses an iterative technique, halting iteration when convergence of each parameter of A is within
C       0.5% of previous value.  Obtains the synthetic spectrum of parameters by sending them to
C       EMI_SPEC which uses NIRS_CONVOLVER to convert synthetic spectrum to what NIRS would
C       measure at each channel.
C
C       MAIN VARIABLES:
C       Y: array of measurements of dimension NCH
C       NPRM: number of parameters to be derived- determines matrix dim's
C                NCH: number of channels in spectrum- determines summation size
C        A: array of derived parameters to be output when iteration is complete
C        SIGMA: array of standard deviations of A parameters
C        F: array of emissions predicted by EMI_SPEC based on inputted parameters, i.e. f(A)
C       DFDX:  array of centered-difference derivatives
C
C       NOTE: the resolution used in the subroutine is set by the parameter RES.  Once convergence
C       occurs to less than RES for all parameters, the loop halts and A is returned.
CCCCCCCCCCCCCCCCCCCCCCCCCCCCCCCCCCCCCCCCCCCCCCCCCCCCCCCCCCCCCC

      PARAMETER (RES=1.0, NPRM=31, N=11, NCH=384, MAXLOOPS=10)

      REAL*8  DFDX(NPRM,NCH),B(NPRM),ARRAY(NPRM,NPRM)
      REAL    Y(NCH),DEL(NPRM),A(NPRM),SIGMA(NPRM),F(NCH)
      REAL    CNT2(NCH),X(NPRM),Y1(NCH),Y2(NCH),DX(NPRM),LINES
      INTEGER INDX(NPRM)
      CHARACTER*1 CONV

      COMMON /OH/ID_OH,DARK,LINES(N)
      LOGICAL*1 FIRST/.TRUE./

      IERR=0
      NCOL = 1
      NLOOPS = 0

C     Initialize parameters for a reasonable first guess

      IF (FIRST) THEN
        OPEN(UNIT=4,FILE='[TSMITH.AURORA.DATA]31PRM.DAT',STATUS='OLD')
         READ(4,*)TIME,CHI,CCDTEMP,LOOP
         READ(4,*)(K,A(I),ERR,I=1,31)
         CLOSE(4)
         FIRST = .FALSE.
      ENDIF

      CALL EMI_SPEC(DT,NCOL,A,0, F)

C       Estimate the accuracy of the observed spectra (photon statistics plus the bias statistics (1.2)).
C       CNT2 is the variance of each channel.

      DO 2 I = 1,NCH
    2 CNT2(I) = (Y(I)+DARK)/15.6 + 1.2
```

```
CCCCCCCCCCCCCCCCCC  MAIN LOOP  CCCCCCCCCCCCCCCCCCCCC

 5    NLOOPS = NLOOPS + 1

C     Calculate the derivative array DX using centered difference method.

      DO 140 I=1,NPRM
        DO 10 J=1,NPRM
10        DX(J)=0.0D0
        DELTA = RES
        DO 100 J=1,2
          DELTA = -DELTA
          DX(I) = A(I) + DELTA

C     Set up derivative arrays so that each element except for needed elements is zero.
C     Dx is +/- 1 R  or  1 K.

          GO TO(12,14,80,80,80,80,80,80,80,80,
     &          80,80,80,16,16,16,17,20,28,28,
     &          21,24,24,25,29,32,33,33,33,16,80),I
12          DX(2) = A(2)                              ! CONTINUUM 1
            GO TO 80
14          DX(1) = A(1)                              ! CONTINUUM 2
            GO TO 80
16          DX(N+6) = A(N+6)                          ! N2IP BANDS
            GO TO 80
17          DX(N+3) = A(N+3)                          !    (1,0)
            DX(N+4) = A(N+4)                          !    (2,1)
            DX(N+5) = A(N+5)                          !    (3,2)
            DX(N+20)= A(N+20)                         !    (4,3)
            GO TO 80
20          DX(N+10) = A(N+10)                        ! O2 ATMOS BANDS
            GO TO 80
21          DX(N+7)  = A(N+7)                         !    (0,1)
            GO TO 80
24          DX(N+13) = A(N+13)                        ! OH BANDS
            GO TO 80
25          DX(N+11) = A(N+11)                        !    (6,2)
            DX(N+12) = A(N+12)                        !    (7,3)
            GO TO 80
28          DX(N+14) = A(N+14)                        ! O2 (1,2)&(2,3) TEMP
            GO TO 80
29          DX(N+8)  = A(N+8)                         !    (1,2)
            DX(N+9) = A(N+9)                          !    (2,3)
            GO TO 80
32          DX(N+16) = A(N+16)                        ! N2IRA BANDS
            DX(N+17) = A(N+17)
            DX(N+18) = A(N+18)
C           DX(N+19) = A(N+19)
C           DX(N+20) = A(N+20)
            GO TO 80
33          DX(N+15) = A(N+15)
80        IF(J.EQ.1) CALL EMI_SPEC(DT,NCOL,DX,I, Y1)
          IF(J.EQ.2) CALL EMI_SPEC(DT,NCOL,DX,I, Y2)
100     CONTINUE

        DO 130 J=1,NCH
130       DFDX(I,J)=(Y2(J)-Y1(J))/(2.0D0*RES)
```

```
140  CONTINUE

       DO 170 I=1,NPRM
         DO 160 J=1,NPRM
           ARRAY(I,J)=0.0D0
           DO 150 K=1,NCH
150          ARRAY(I,J)=ARRAY(I,J)+
     &          DFDX(I,K)*DFDX(J,K)/CNT2(K)
160        CONTINUE
         B(I)=0.0D0
         DO 165 L=1,NCH
165        B(I)=B(I)+(Y(L)-F(L))*DFDX(I,L)/CNT2(L)
170      CONTINUE

C        Invert ARRAY matrix, then solve for X=ARRAY*B

       CALL MATINV(ARRAY,NPRM,NPRM)

       DO 550 I=1,NPRM
         X(I) = 0.0D0
         DO 500 J=1,NPRM
500        X(I) = X(I) + ARRAY(I,J)*B(J)
         DEL(I) = X(I)                          ! For use in convergence test
         A(I) = X(I) + A(I)                     ! SOLVE for a(i) for use in next iteration
550    CONTINUE

C        Calculate error of each parameter

       DO 580 I=1,NPRM
       IF(ARRAY(I,I).GE.0.0D0)
     &    SIGMA(I)=SQRT(ARRAY(I,I))
       IF(A(I).LT.1.0E-5) THEN
         DEL(I) = 0.0
         A(I)=1.0
       ENDIF
580  CONTINUE

C        Calculate error-weighted Chi-squared

       CALL EMI_SPEC(DT,NCOL,A,0, F)
       XSI = 0.0
       DO I = 1, NCH
        XSI = XSI + (Y(I)-F(I))**2/CNT2(I)
       ENDDO
       XSI = XSI/(NCH-NPRM)

C        Now test each parameter for convergence using 0.05% as criterion.  Repeat loop if convergence
C        has not occurred (for parameters w/ magnitude > 100) unless MAXLOOPS iterations have
C        occurred.

       CONV = 'Y'
       DO 600 I=1,NPRM
600      IF (ABS(DEL(I)/A(I)).GE.0.005 .AND.
     &          A(I).GE.100.) CONV='N'
         IF (NLOOPS.LT.MAXLOOPS .AND.
     &          CONV.EQ.'N') GOTO 5
999  RETURN
       END
```

```
CCCCCCCCCCCCCCCCCCCCC  SUBROUTINE EMI_SPEC  CCCCCCCCCCCCCCCCCCCCC

      SUBROUTINE EMI_SPEC(DT,NCOL,A,IST, EMI)

C       PURPOSE:
C       To calculate an emission spectrum based on A parameters that can be used to compare with a
C       measurement from the NIRS instrument.  Emission spectrum is sent to NIRS_CONVOLVER
C       subroutine to convert thousands of atomic and molecular lines to a channel-by-channel signal.
C
C       MAIN VARIABLES:
C       NCOL:  number of pixels per column, or channel, set on the CCD at measurement time.
C       W:  array of wavelengths returned from band models
C       WLT:  array of wavelenghts of all emission lines
C       S:  array of strengths returned from band models
C       STR:  array of strengths of all emission lines
C       NUM1:  number of lines returned from a band model
C       NUM:  total number of lines to be convolved

      PARAMETER (NCH=384, NPRM=31, N=11, MAXLN=10000)
      REAL    LINES,A(NPRM),EMI(NCH),W1(200),W2(200)
      REAL*8  WAVE,W(1500),S(1500),WLT(MAXLN),STR(MAXLN)
      COMMON /OH/ID,DARK,LINES(N)

C       Call the appropriate band model(s) given by the IST indicator

      ISTEP=IST+1
      NUMTOT=0
       GO TO(11,90,90,90,90,90,90,90,90,90,
     &       90,90,90,90,11,12,13,11,21,22,
     &       23,21,31,32,31,22,41,41,42,43,
     &       14,52),ISTEP

  11    CALL N21P(1,0,A(N+6),W,S,NUM1)
        CALL ADDLIN(N+3,1,NUM1,NUMTOT,W,S,A, WLT,STR)
        IF (ISTEP.NE.1 .AND. ISTEP.NE.N+7) GO TO 90
  12    CALL N21P(2,1,A(N+6),W,S,NUM1)
        CALL ADDLIN(N+4,1,NUM1,NUMTOT,W,S,A, WLT,STR)
        IF (ISTEP.NE.1 .AND. ISTEP.NE.N+7) GO TO 90
  13    CALL N21P(3,2,A(N+6),W,S,NUM1)
        CALL ADDLIN(N+5,1,NUM1,NUMTOT,W,S,A, WLT,STR)
        IF (ISTEP.NE.1 .AND. ISTEP.NE.N+7) GO TO 90
  14    CALL N21P(4,3,A(N+6),W,S,NUM1)
        CALL ADDLIN(N+19,1,NUM1,NUMTOT,W,S,A, WLT,STR)
        IF (ISTEP.NE.1) GO TO 90

  21    CALL ATMOS_CROSS(0,1,1,A(N+10),W,S,W1,W2,NUM1)
        CALL ADDLIN(N+7,1,NUM1,NUMTOT,W,S,A, WLT,STR)
        IF (ISTEP.NE.1) GO TO 90
  22    CALL ATMOS_CROSS(1,2,1,A(N+14),W,S,W1,W2,NUM1)
        CALL ADDLIN(N+8,1,NUM1,NUMTOT,W,S,A, WLT,STR)
        IF (ISTEP.NE.1 .AND. ISTEP.NE.N+15) GO TO 90
  23    CALL ATMOS_CROSS(2,3,1,A(N+14),W,S,W1,W2,NUM1)
        CALL ADDLIN(N+9,1,NUM1,NUMTOT,W,S,A, WLT,STR)
        IF (ISTEP.NE.1) GO TO 90

  31    CALL OH_SPEC(6,2,A(N+11),A(N+13),ID, W,S,NUM1)
        CALL ADDLIN(N+11,2,NUM1,NUMTOT,W,S,A, WLT,STR)
```

```
      IF (ISTEP.NE.1 .AND. ISTEP.NE.N+14) GO TO 90
32    CALL OH_SPEC1(7,3,A(N+12),A(N+13),ID, W,S,NUM1)
      CALL ADDLIN(N+12,2,NUM1,NUMTOT,W,S,A, WLT,STR)
      IF (ISTEP.NE.1) GO TO 90

41    CALL BANDSYN(6,A(N+16),A(N+15),11,6,W,S,NUM1)
      CALL ADDLIN(N+16,3,NUM1,NUMTOT,W,S,A, WLT,STR)
      IF (ISTEP.NE.1 .AND. ISTEP.NE.N+16) GO TO 90
42    CALL BANDSYN(6,A(N+17),A(N+15),6,2,W,S,NUM1)
      CALL ADDLIN(N+17,3,NUM1,NUMTOT,W,S,A, WLT,STR)
      IF (ISTEP.NE.1 .AND. ISTEP.NE.N+16) GO TO 90
43    CALL BANDSYN(6,A(N+18),A(N+15),12,7,W,S,NUM1)
      CALL ADDLIN(N+18,3,NUM1,NUMTOT,W,S,A, WLT,STR)
      IF (ISTEP.NE.1) GO TO 90

51    CALL BANDSYN(5,A(N+20),500.0,4,2,W,S,NUM1)
      CALL ADDLIN(N+20,3,NUM1,NUMTOT,W,S,A, WLT,STR)
      IF (ISTEP.NE.1) GO TO 90
52    CALL BANDSYN(5,A(N+21,500.0,5,3,W,S,NUM1)
      CALL ADDLIN(N+20,3,NUM1,NUMTOT,W,S,A, WLT,STR)
90    CONTINUE

C     Now add the atomic lines to the WLT and STR arrays then convolve the arrays into a channel-by-
C     channel signal.

      DO I=1,N
       WLT(NUMTOT+I)  = LINES(I)
       STR(NUMTOT+I) = A(I+2)
      ENDDO
      NUM = NUMTOT + N
      CALL NIRS_CONVOLVER(WLT,STR,NUM,A(1),A(2),NCOL,DT, EMI)
      RETURN
      END


CCCCCCCCCCCCCCCCCCCCC   SUBROUTINE ADDLIN   CCCCCCCCCCCCCCCCCCCCCC

      SUBROUTINE ADDLIN(II,OHFLAG,NUM1,NUMTOT,W,S,A, WLT,STR)

C     PURPOSE:
C     Adds emission lines from the W and S arrays to the WLT and STR arrays respectively, but first
C     convert the different strengths given by the different band models to a band brightness
C     normalization if necessary.
C
CCCCCCCCCCCCCCCCCCCCCCCCCCCCCCCCCCCCCCCCCCCCCCCCCCCCCCCCCCCCCC

      PARAMETER (NPRM=31, MAXLN=10000)
       INTEGER OHFLAG
       REAL A(NPRM)
       REAL*8 W(1500),S(1500),WLT(MAXLN),STR(MAXLN)

      GO TO (10,20,30),OHFLAG
10     DO 15 I=1,NUM1
        WLT(NUMTOT+I) = W(I)
15      STR(NUMTOT+I) = S(I)*A(II)
      GO TO 40
20     DO 25 I=1,NUM1
        WLT(NUMTOT+I) = 1.0D3/(1.000275D-5*W(I))
```

```
25       STR(NUMTOT+I) = S(I)
      GO TO 40
30     DO 35 I=1,NUM1
        WLT(NUMTOT+I) = W(I)
35       STR(NUMTOT+I) = S(I)
40   CONTINUE
     NUMTOT = NUMTOT + NUM1
     RETURN
     END


CCCCCCCCCCCCCCCC   SUBROUTINE NIRS_CONVOLVER   CCCCCCCCCCCCCCCCCCCCCC

     SUBROUTINE NIRS_CONVOLVER(WAVEL,B,NUM,CON1,CON2,NCOL,DT, SIG)

C        PURPOSE:
C        Takes input of wavelengths, their associated line strengths, and high and low continuum and
C        convolves the lines into a channel-by-channel signal that would be measured by the NIRS
C        instrument.
C
C     DESIGNED BY JENG-HWA YEE
C     WRITTEN BY JENG-HWA YEE
C
C      DATE= OCT 2, 1990
CCCCCCCCCCCCCCCCCCCCCCCCCCCCCCCCCCCCCCCCCCCCCCCCCCCCCCCCCCCCCCCCCC

       PARAMETER (MAXLN=10000, NCH=384)

       REAL*8 WAVE,WAVEL(MAXLN),B(MAXLN)
        DIMENSION SPEC(500),SPEC_P(500)
       DIMENSION SIGNAL(NCH),SIG(NCH)
       DIMENSION TR(27),SEN(NCH)
        LOGICAL*1 FIRST_CALL/.TRUE./

     DATA AD_UNIT/15.6/
     COMMON /TRANS/WAVE

     IF (FIRST_CALL) THEN
      OPEN(UNIT=11,FILE='[TSMITH.AURORA.DATA]MATIS_INST_01_91.DAT',
   &     READONLY,SHARED,STATUS='OLD')
      OPEN(UNIT=12,FILE='[TSMITH.AURORA.DATA]MATIS_SENS_01_91.DAT',
   &     READONLY,SHARED,STATUS='OLD')

       DO J = 1,27
        READ(11,*) TR(J)
       ENDDO

       DO L = 1,NCH
        READ(12,*) WAVELE,SEN(L),SENS_ERR
       ENDDO

       DW_DP = 1.4035
       DW = DW_DP*1.0E8/(WAVE-100.0)**2
       TOT = 0.0
       DO I = 1,27
        TOT = TOT + TR(I)*DW_DP
       ENDDO
```

```
  FIRST_CALL = .FALSE.
ENDIF

SLOPE = (CON2-CON1)/FLOAT(NCH)

DO L = 1,500
  SPEC(L) = (CON1+ (L-50)*SLOPE)*DW
ENDDO

DO L = 1,NUM
  II = (WAVE - WAVEL(L))/DW_DP + 50
  IF (II.LE.500 .AND.II.GE.0) SPEC(II) = SPEC(II) + B(L)
ENDDO

DO L = 1,NCH
  SIGNAL(L) = 0.0
  SPEC_P(L) = 0.0
ENDDO

DO I = 1,NCH
  II = I + 50
  DO J = 1,27
    SPEC_P(I) = SPEC_P(I) + TRO(J)*SPEC(II-14+J)
  ENDDO
ENDDO

DO L = 1,NCH
  II = (L-1)*NCOL + 1
  DO I = II, II+NCOL-1
    SIGNAL(L) = SIGNAL(L) + SPEC_P(I)
  ENDDO
ENDDO
DO N = 1,NCH
 SIG(N)=SEN(N)*SIGNAL(N)*DT/(TOT*NCOL)
ENDDO
RETURN
END
```

BIBLIOGRAPHY

Bates, D. R., and M. Nicolet, The Photochemistry of Atmospheric Water Vapor, *J. Geophys. Res.*, 55, 301, 1950.

Bevington, P. R., *Data Reduction and Error Analysis for the Physical Sciences*, Mcgraw-Hill, New York, 1969.

Cartwright, D. C., S. Trajmar, and W. Williams, Vibrational Population of the $A^3\Sigma_u^+$ and $B^3\Pi_g$ States of N_2 in Normal Auroras, *J. Geophys. Res.*, 76, 8368, 1971.

Chapman, S., Auroral Science, 1600 to 1965 Towards it's Golden Age?, in *Atmospheric Emissions* by B. M. McCormac and A. Omholt (eds.), Van Nostrand Reinhold, New York, 1969.

Gattinger, R. L., and A. Vallance Jones, Quantitative Spectroscopy of the Aurora. II. The Spectrum of Medium Intensity Aurora Between 4500 and 8900 Å, *Can. J. Phys.*, 52, 2343, 1974.

Herzberg, G., *Atomic Spectra and Atomic Structure*, Dover Publications, New York, 1945.

Huber, K. P., and G Herzberg, *Molecular Spectra and Molecular Structure, IV. Constants of Diatomic Molecules*, Van Nostrand Reinhold, New York, 1979.

Hedin, A. E., MSIS-86 Thermospheric Model, *J. Geophys. Res.*, 92, 4649, 1987.

Jursa, A. S., *Handbook of Geophysics and the Space Environment*, Air Force Geophysics Laboratory; National Technical Information Service, Springfield, VA, 1985.

Killeen, T. L., and P. B. Hays, Doppler Line Profile Analysis for a Multi-channel Fabry-Perot Interferometer, *J. Appl. Optics*, 23, 612, 1984.

Krupenie, P. H., The Spectrum of Molecular Oxygen, *J. Chem. Ref. Data*, 1, 423, 1972.

Lofthus, A. and P. H. Krupenie, The Spectrum of Molecular Nitrogen, *J. Chem. Ref. Data*, 6, 113, 1977.

Moore, C. E., A Multiplet Table of Astrophysical Interest, *Contrib. Princeton Univ. Obs.*, No. 20, 1945.

Rees, M. H., *Physics and Chemistry of the Upper Atmosphere*, Cambridge University Press, Cambridge, Great Britain, 1989.

Schadee, A., The Formation of Molecular Lines in the Solar Spectrum, *Bul. Astr. Inst. Neth.*, 17, 325, 1964.

Starkov, G. V., and Y. I. Feldstein, Auroral Oval and it's Dependence on Magnetic Disturbance, Results of Researches on the Inbternational Geophys. Profects Pub. House 'NAUK', Moscow, Articles, *Polar Aurora,* 17, 22.

Vallance Jones, A., *Aurora*, D. Reidel Publishing Co., Dordrecht, Holland, 1974.

Weast, R. C., *CRC Handbook of Chemistry and Physics*, CRC Press, Boca Raton, Florida, 1988.

Whalen, B. A., D. W. Green, and I. B. McDiarmid, Observations of Ionospheric Ion Flow and Related Convective Electric Fields in and near an Auroral Arc, *J. Geophys. Res.*, 79, 2835, 1974.

Wiese, W. L., M. W. Smith, and B. M. Glennon, *Atomic Transition Probabilities Vol. I Hydrogen through Neon*, National Bureau of Standards, Washington, D. C., 1966.

Yee, J. H., R. Niciejewski, and M. Z. Luo, Observations of $O_2(^1\Sigma)$ and OH Nightglow During the Aloha-90 Campaign, *J. Geophys. Res.*, 18, 1357, 1991.